Structural and Multidisciplinary Optimization (2019) 59:2227–2255
https://doi.org/10.1007/s00158-018-02189-0

RESEARCH PAPER

Tension/compression anisotropy enhanced topology design

Georgios Gaganelis[1] · Dustin Roman Jantos[2] · Peter Mark[1] · Philipp Junker[2]

Received: 14 June 2018 / Revised: 18 December 2018 / Accepted: 26 December 2018 / Published online: 15 February 2019

Abstract
A strategy for tension/compression anisotropy enhancement of topology optimization approaches is presented. To this end, a spectral decomposition of stresses and strains into tension and compression contributions allows for a multi-material optimization that favors tension or compression affine materials, dependent on the predominant local state. Numerical computations hence yield the topology of a construction part with maximum stiffness at constraint design volume. Additionally, the spatial distribution of a tension affine and a compression affine material is optimized, which is motivated by concrete engineering: financially cheap material, for example concrete, is applied in compression dominant regions in favor of stiffer but more expensive material, which is applied only in tension dominant regions, for example steel. The enhancement is applied both to a classical (mathematical) optimization method and the thermodynamic topology optimization. Several numerical examples are investigated and yield design suggestions for tension/compression sensitive construction parts, e.g., for future lightweight structures made of reinforced concrete.

Keywords Multi-material topology optimization · Tension/compression anisotropy · MRM · Thermodynamic topology optimization

1 Introduction

Structural topology optimization has become a popular tool in engineering within recent years, cf. Sigmund and Maute (2013). In most cases, no distinction between tension and compression states is made which might be sufficient for many engineering applications, e.g., for steel structures. Steel is a prominent example for materials with similar strength both under tension and compression. However, in some cases, a more sophisticated optimization is desired, i.e., when materials are considered which show a strong anisotropic failure behavior. For example, in concrete engineering, the distinction of structural components being subjected to compressive or tensile stresses is of great importance for the principle design. Generally, concrete has a high compressive but only poor tensile strength of which the latter usually is treated as zero in structural design within concrete engineering. To be able to bear tensile stresses, a concrete structure therefore has to be reinforced with steel what leads to reinforced concrete (RC). As mentioned, steel has a comparable behavior in both compression and tension but exhibits the disadvantages of high mass and costs compared to concrete. Furthermore, actions against corrosion have to be taken into account. Consequently, a mechanically efficient and economically favorable load-bearing structure in terms of concrete engineering should be designed in a way that compression is taken by concrete whereas reinforcement steel should be limited to bear tensile stresses.

Several works tackle the problem of tension/compression anisotropy during the optimization process. Minimum weight optimization under compliance and (local) stress constraint approaches can provide different yield strengths under tension and compression by applying the Drucker-Prager stress criterion (Bruggi and Duysinx 2012; Luo and Kang 2012), which can be extended to multi-material

Responsible Editor: Seonho Cho

✉ Georgios Gaganelis
georgios.gaganelis@rub.de

[1] Institute of Concrete Structures, Ruhr University Bochum, Bochum, Germany

[2] Institute of Mechanics of Materials, Ruhr University Bochum, Bochum, Germany

topology optimization (Luo et al. 2012). Another common method is to define the spatial distribution of tension and compression affine material with respect to the spectral decomposition of local stresses and/or strains while maximizing the structural stiffness under volume constraint. An approach for truss structures can be found in Martinez et al. (2007) which is based on a sequential topology, size, and shape optimization algorithm. The results coincide with analytical solutions. Truss-like continua are optimized in Querin et al. (2010): the material applied in the finite element (FE) analysis is an orthotropic mixture of two different linear elastic isotropic materials. The resulting stresses are transformed into principal directions and either of the two materials is applied in each direction depending on the sign of the principal stresses in those directions. In Liu and Qiao (2011), a similar orthotropic mixture is used but enhanced by a modified Heaviside function for a smoothed interpolation between the elastic properties of two different linear elastic isotropic materials. Additionally, optional price functions for the materials are introduced to optimize the financial costs or to reduce the weight of the structure. A rather simple to implement but efficient approach is given in Cai (2011) referred to as the material-replacement method (MRM). The material stiffness is modified by a weight function considering the signs of the principal stresses. The original approach includes only a single material which is either considered as so-called "compression-only" or "tension-only". The method was extended to multiple bi-modulus materials in Cai et al. (2016), i.e., materials with different elasticity moduli in compression and tension, by approximating each bi-modulus material with two isotropic materials. In each iteration of the optimization process the real material's modulus is chosen between the two substituting materials in dependence of the current stress state.

The current publication aims at proceeding one step further and presents a strategy based on the work of Cai (2011). The spectral decomposition of the (local) stresses and strains into their tensile and compressive parts provides an energetical decomposition in tension and compression, which is used for indirect consideration of anisotropic material affinities, yet without including the actual nonlinearity of materials within FE analysis. To this end, a three-phase system is introduced consisting of void, one material with affinity to tension (e.g., steel) and one to compression (e.g., concrete), respectively. Two design variables are considered for the compliance minimization under volume constraint: a density variable for the topology of the structure defining whether there is material or void and a phase variable defining which of the two non-void materials spatially forms the structure. A SIMP approach is used for the density variable whereas the phase distribution is determined by the local decomposition of the elastic energy in tension and compression: one material is applied in tension dominant regions and the other in compression dominant regions to mimic the usual design approach in concrete engineering. To demonstrate the broad applicability of the presented procedure, it is employed to two different approaches: the material-replacement method (referred to as MRM) and the thermodynamic topology optimization (referred to as TDO).

The MRM is expanded to multi-phase optimization: the sensitivities are modified by a weight function considering the decomposed elastic energy into tension and compression to provide the respective affinity of the materials. The optimization algorithm is based on the implementation given in Andreassen et al. (2011) including a sensitivity filter and the method of moving asymptotes (MMA) (Svanberg 1987) as solver. The topology and phase distribution are updated simultaneously within the optimization iteration.

The TDO was introduced first in Junker and Hackl (2015) and progressively improved in Junker and Hackl (2016), Jantos et al. (2016, 2018a). In contrast to classical optimization, the optimization process follows from Hamilton's principle which is widely used for variational material modeling. This principle demands the formulation of the Gibbs energy and a dissipative functional, whose sum is assumed to be stationary with respect to all governing variables. These variables, which are the same as for the MRM, are the displacement field, the density variable and the phase variable for the tension and compression affine material. For regularization of the problem, a gradient-enhancement based on finite differences is employed, see Jantos et al. (2018a) and Junker et al. (2019). Hamilton's principle then yields as stationarity condition an ordinary/partial differential equation (ODE/PDE) for each design variable, which is referred to as evolution equation in the context of material modeling. They serve as design update, which can be evaluated simultaneously within an iterative optimization algorithm. An energetic penalization is introduced to account for the tensile and compressive affinity of the materials.

The paper begins with some preliminaries to the tension/compression anisotropy enhancement for topology optimization. After the presentation of the derivation and numerical treatment of the tension/compression anisotropy enhanced MRM and TDO, a comparative analysis of the respective mathematical structure is given. Afterwards, several boundary value problems are solved

whose numerical results serve as basis for comparison. Although this publication focuses on single load cases, examples for multiple load cases are also presented. Finally, an example for practical application in the field of structural concrete design is presented.

2 Tension/compression anisotropy enhancement

The following preliminaries serve as general basis and will be applied to both approaches to topology optimization (MRM and TDO). To enhance topology optimization approaches by tension/compression anisotropy, the classical spectral decomposition of the stresses and strains is adopted. This procedure was also used by Cai (2011) to derive the MRM and is known for instance in the context of damage mechanics as well, cf. Voyiadjis et al. (2008). The stress is hence decomposed into

$$\boldsymbol{\sigma} = \boldsymbol{\sigma}_+ + \boldsymbol{\sigma}_- \tag{1}$$

with

$$\boldsymbol{\sigma}_+ = \sum_{i=1}^{3} \sigma_i \boldsymbol{e}_i \otimes \boldsymbol{e}_i \quad \forall \quad \sigma_i > 0, \qquad \boldsymbol{\sigma}_- = \sum_{i=1}^{3} \sigma_i \boldsymbol{e}_i \otimes \boldsymbol{e}_i \quad \forall \quad \sigma_i < 0 \tag{2}$$

where σ_i denote the (scalar) principal stresses or equivalently the eigenvalues of $\boldsymbol{\sigma}$. The spectral decomposition of the strains analogously reads as

$$\boldsymbol{\varepsilon} = \boldsymbol{\varepsilon}_+ + \boldsymbol{\varepsilon}_- \tag{3}$$

with

$$\boldsymbol{\varepsilon}_+ = \sum_{i=1}^{3} \varepsilon_i \boldsymbol{e}_i \otimes \boldsymbol{e}_i \quad \forall \quad \varepsilon_i > 0, \qquad \boldsymbol{\varepsilon}_- = \sum_{i=1}^{3} \varepsilon_i \boldsymbol{e}_i \otimes \boldsymbol{e}_i \quad \forall \quad \varepsilon_i < 0 \tag{4}$$

where ε_i denotes the (scalar) principal strains or equivalently the eigenvalues of $\boldsymbol{\varepsilon}$. For using an energetic measure of the tension/compression anisotropy, the potential energy (which is equivalent to the Helmholtz free energy) will be utilized, defined by

$$\Pi := \frac{1}{2} \boldsymbol{\sigma} : \boldsymbol{\varepsilon} \, . \tag{5}$$

Inserting the spectral decomposition given in (1) and (3) into the potential energy yields

$$\Pi = \underbrace{\frac{1}{2} \boldsymbol{\sigma}_+ : \boldsymbol{\varepsilon}_+}_{:=\Pi_+} + \underbrace{\frac{1}{2} \boldsymbol{\sigma}_- : \boldsymbol{\varepsilon}_-}_{:=\Pi_-} + \underbrace{\frac{1}{2} \boldsymbol{\sigma}_+ : \boldsymbol{\varepsilon}_- + \frac{1}{2} \boldsymbol{\sigma}_- : \boldsymbol{\varepsilon}_+}_{:=\Pi_{+-}} \, . \tag{6}$$

with $\Pi_{+-} = 0$ for isotropic materials. Similarly to Cai et al. (2016), the relative energy amount imposed by compression loads is defined by

$$R_- := \frac{\Pi_-}{\Pi} \tag{7}$$

and the relative energy amount imposed by tension loads by

$$R_+ := \frac{\Pi_+}{\Pi} \, . \tag{8}$$

It thus immediately follows

$$R_+ + R_- = 1 \qquad \Leftrightarrow \qquad R_+ = 1 - R_- \, . \tag{9}$$

It will be shown in the following sections that this energetic decomposition is sufficient for tension/compression anisotropy enhancement. To be more precise, the "measures" for tension/compression anisotropy R_- and $R_+ = 1 - R_-$ can be implemented into existing approaches to topology optimization in two different ways: they might be used by an enhancement of the stiffness matrix to calculate modified sensitivities as will be done for the MRM approach; or by an enhancement of an energetic penalization term as will be done for the TDO approach.

3 Extended bi-material-replacement method

3.1 Preliminaries

The classical minimum compliance problem subject to a volume constraint, see e.g., Bendsøe and Kikuchi (1988) and Bendsøe (1989), serves as basis for the tension/compression anisotropy enhancement of the MRM. It is stated as follows: given a feasible design space Ω that is discretized by N_e finite elements, the purpose is to minimize the objective function, which is the mean structural compliance

$$c := \hat{\boldsymbol{U}}^T \cdot \boldsymbol{K} \cdot \hat{\boldsymbol{U}} \, , \tag{10}$$

while the structural volume V is limited to a predefined ratio

$$\varrho = \frac{V}{\Omega} \,. \tag{11}$$

The following notations are introduced regarding the discretization: quantities discretized at the nodes of the FE mesh are denoted by $\hat{(\cdot)}$ whereas quantities discretized at the integration (Gauß) points are denoted by $\tilde{(\cdot)}$. Element-wise constant quantities are denoted by $\bar{(\cdot)}$. In (10) $\hat{\boldsymbol{U}}$ and $\boldsymbol{K}$ are the global (= assembled) displacement vector and global stiffness matrix, respectively. The displacement vector for each element e is denoted by $\hat{\boldsymbol{u}}_e$ and the corresponding stiffness matrix by $\bar{\boldsymbol{k}}_e$. To link the statical FE setting with the optimization problem, the three-phase SIMP interpolation scheme (Sigmund 2001b) is utilized, whereby one phase is void. Herein, two design variables $\bar{\chi}$ and $\bar{\varphi}$ are discretized element-wise and define each element stiffness matrix $\bar{\boldsymbol{k}}$ as

$$\bar{\boldsymbol{k}}(\bar{\chi}, \bar{\varphi}) = \bar{\chi}^p \, \left[\bar{\varphi}\, \bar{\boldsymbol{k}}_- + (1-\bar{\varphi})\, \bar{\boldsymbol{k}}_+\right] \tag{12}$$

where $\bar{\chi}$ is the well-known "relative density" and $\bar{\varphi}$ a second design variable which interpolates between the two predefined materials represented by their element stiffness matrix $\bar{\boldsymbol{k}}_-$ and $\bar{\boldsymbol{k}}_+$, respectively. For $\bar{\chi} = 0$, the element is "void" and for $\bar{\chi} = 1$, it is "solid", i.e., there is none or full material. Because of the well-known difficulties that arise from a discrete valued optimization problem, mathematical relaxation is applied on the design variables so that any value in the interval [0, 1] is feasible. To avoid thereof emerging hard to interpret intermediate ("gray") densities, i.e. $\bar{\chi} \in [0, 1]$, the usual penalty power p is used. A reasonable value for the penalization can be justified and derived physically as a function of the Poisson's ratio (Bendsøe and Sigmund 1999) and is usually set to $p = 3$. The element stiffness is composed additively of the isotropic stiffness matrices $\bar{\boldsymbol{k}}_-$ and $\bar{\boldsymbol{k}}_+$ that are assigned to the predefined compressive material "−" and the tensile material "+" , respectively. The additive composition may be interpreted as an upper Voigt bound of the energy. The single-material proportions are steered by the continuous phase variable $\bar{\varphi}$, in which $\bar{\varphi} = 0$ denotes full tensile material and $\bar{\varphi} = 1$ full compressive material. Although a second penalty power for the phase variable could be applied to push $\bar{\varphi}$ towards a 0–1 distribution in order to avoid "hybrid" elements consisting of two materials, this would lead to physical inconsistency because for an exponent larger than 1, the sum of the material proportions could become < 1. Hence, no penalty power for the phase variable is used. The "hybrid" element problem will be overcome later by taking into account the tensile and compressive anisotropy of materials. The optimization problem can be formulated as

$$\begin{aligned}
&\text{find: } \bar{\boldsymbol{\chi}} = [\bar{\chi}_1, \bar{\chi}_2, ..., \bar{\chi}_{N_e}]^T \,,\ \bar{\boldsymbol{\varphi}} = [\bar{\varphi}_1, \bar{\varphi}_2, ..., \bar{\varphi}_{N_e}]^T \\
&\text{such that } c(\bar{\boldsymbol{\chi}}, \bar{\boldsymbol{\varphi}}) = \hat{\boldsymbol{U}}^T \cdot \boldsymbol{K}(\bar{\boldsymbol{\chi}}, \bar{\boldsymbol{\varphi}}) \cdot \hat{\boldsymbol{U}} \\
&\qquad\qquad = \sum_{e=1}^{N_e} \hat{\boldsymbol{u}}_e^T \cdot \bar{\boldsymbol{k}}_e(\bar{\chi}_e, \bar{\varphi}_e) \cdot \hat{\boldsymbol{u}}_e \rightarrow \min_{\bar{\boldsymbol{\chi}}, \bar{\boldsymbol{\varphi}}} \\
&\text{subject to: } f(\bar{\boldsymbol{\chi}}) = V(\bar{\boldsymbol{\chi}}) - \varrho\, \Omega = \sum_{e=1}^{N_e} \Omega_e \bar{\chi}_e - \varrho \sum_{e=1}^{N_e} \Omega_e \leq 0 \,, \\
&\qquad\qquad \boldsymbol{K}(\bar{\boldsymbol{\chi}}, \bar{\boldsymbol{\varphi}}) \cdot \hat{\boldsymbol{U}} = \boldsymbol{F} \,, \\
&\qquad\qquad 0 \leq \chi_{\min} \leq \chi_e \leq 1 \,, \\
&\qquad\qquad 0 \leq \varphi_e \leq 1 \,.
\end{aligned} \tag{13}$$

The quantity Ω_e is the element volume and ϱ is the volume fraction of the optimized structure subject to the total volume of the initial design space Ω. The parameter $\chi_{\min}$ is a lower, nonzero bound to avoid singularity within the FE computations. It should be mentioned that the formulation can be modified, for instance the objective and constraint function can be interchanged. Also the volume constraint can be formulated more elaborated, considering for example material weight. Such a mass-related constraint can be written as

$$M(\bar{\boldsymbol{\chi}}, \bar{\boldsymbol{\varphi}}) - \varrho_M\, M_0 = \sum_{e=1}^{N_e} \bar{\chi}_e\, \Omega_e [\bar{\varphi}_e\, \rho_- + (1-\bar{\varphi}_e)\, \rho_+] - \varrho_M\, M_0 \leq 0 \tag{14}$$

where ρ_+ and ρ_- are the (given) mass densities of the tension affine material and compression affine material, respectively, and ϱ_M is the ratio of the optimized structure mass to that of the initial material distribution. However, the results presented in this paper correspond to the formulation given in (13).

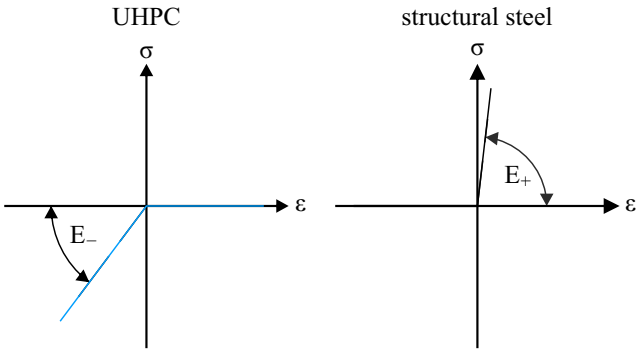

Fig. 1 Approximated stress/strain relations used in the presented bi-material MRM approach

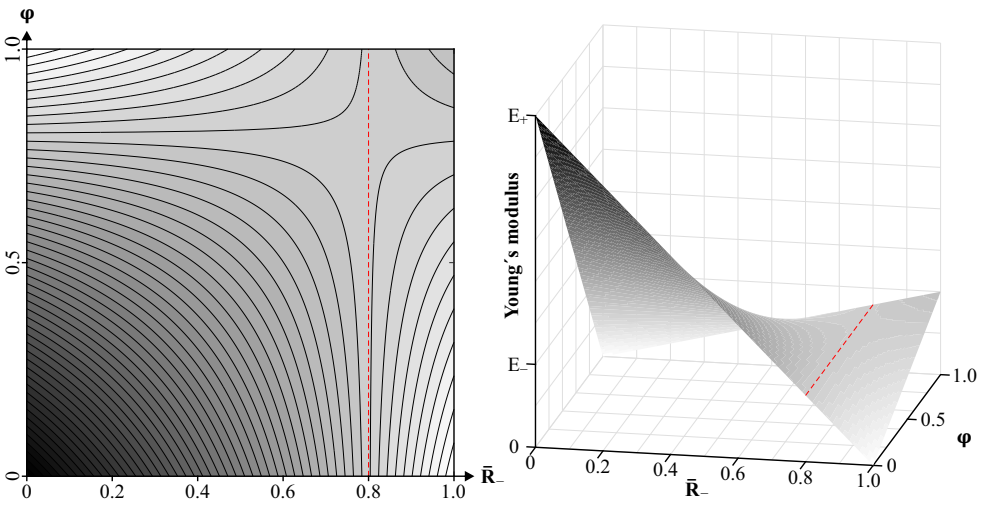

Fig. 2 Left: contour plot of the element phase variable $\bar{\varphi}$ over the modification factor $\bar{R}_-$ subject to the element stiffness (isolines) in terms of the element's modified Young's modulus, for a fixed $\bar{\chi}^p$ and $E_+/E_- = 4$. Right: three-dimensional visualization of the interrelations

3.2 Tension/compression anisotropy enhancement by stiffness modification

To take into account the tension and compression affinity of the two materials, generally the stress/strain relationship has to be represented in the FE model. For a realistic representation of the stress/strain relation of many materials, like for example ultra high-performance concrete (UHPC) and steel, this implies a nonlinear approach. Considering the several nonlinear structural reanalysis within each optimization iteration and also a more cumbersome sensitivity analysis, it leads to remarkable, high computational costs. To prevent this drawback, Cai (2011) proposes the material-replacement method (MRM) as an approach to introduce so-called "tension-only" or "compression-only" materials in the single-material topology optimization procedure yet within a linear FE analysis. For suitable boundary conditions MRM thus yields structures purely under compression or tension depending on the predefined material, i.e., compression-only or tension-only, respectively. The respective material is herein replaced by a linear elastically behaving, isotropic material with equal elasticity properties, i.e. Young's modulus and Poisson's ratio, in both compression and tension. Subsequently, the real behavior of the anisotropic material is approximated gradually in each iteration by modifying the element stiffnesses depending on their respective local stress state. The simplified adoption of a linear elastic, isotropic material utilized to calculate deformations, strains, and stresses in the FE analysis is "corrected" subsequently, i.e., the element stiffness for the optimization process is altered depending on the local stress state:

$$\bar{\boldsymbol{k}}_R = \bar{R}^{\star}_{\pm}\,\bar{\boldsymbol{k}}\,. \tag{15}$$

In (15), $\bar{\boldsymbol{k}}_R$ is the modified element stiffness matrix and $\bar{R}^{\star}_{\pm} = \{\bar{R}^{\star}_{+}, \bar{R}^{\star}_{-}\}$ is the affiliated element modification factor defined as

$$R^{\star}_{+} = \max\left\{R_{\min}, \frac{\Pi_+}{\Pi}\right\} \quad \text{and} \quad R^{\star}_{-} = \max\left\{R_{\min}, \frac{\Pi_-}{\Pi}\right\} \tag{16}$$

for the tension affine "+" and compression affine "−" material, respectively. Obviously, it holds $\bar{R}^{\star}_{-} = \bar{R}_-$ according to (7) for $\Pi_-/\Pi > R_{\min}$. $R_{\min}$ is a lower bound to avoid singularity, e.g., $R_{\min} = 10^{-6}$. In order to simplify the notation, we are going to use $\bar{R}_+ = \bar{R}^{\star}_{+}$ and $\bar{R}_- = \bar{R}^{\star}_{-}$,

Fig. 3 Results for the Messerschmidt-Bölkow-Blohm (MBB) beam with sensitivity filter (left) for phase variable and without (right)

respectively. In a numerical implementation, the element stiffness is modified individually in each iteration step after firstly computing the principal stresses and strains for an isotropic material behavior and subsequently "correct" the assumption by modifying the local stiffness based on the local stress state. To be more precise, we emphasize that according to Cai (2011) both the unmodified $\bar{\boldsymbol{k}}$, cf. (12), and the modified $\bar{\boldsymbol{k}}_R$ stiffness matrix, cf. (15), are applied in each iteration: the unmodified for the FE calculations representing the linear elastic isotropic "replacing material" and the modified to alter the sensitivities needed to update the design variables. Hence, the method operates somehow heuristic to enhance tension- or compression-only materials within a linear FE framework by solving a subproblem. As will be demonstrated by the numerical results, this strategy still yields very reasonable optimization results.

The single-material MRM approach has been extended to a multi-material framework (Cai et al. 2016). Motivated to design lightweight structures through the intelligent application of materials, regarding the existing multi-material MRM approach some difficulties arise. In Cai et al. (2016) the considered materials are so-called bi-modulus, i.e., they exhibit a different behavior in tension and compression, respectively. While each bi-modulus material is composed of two isotropic materials with Young's modulus according to the tensile and compressive stiffness, the FE computation is carried out with either the compensatory tensile or compressive material. Hence, the method is based on switching between the two predefined virtual materials for each bi-modulus and interpolate then between the two corresponding compensatory tensile or compressive replacing materials, respectively, of each real compression affine and tension affine material. In doing so, the choice of material and thus the optimization results strongly depend on the predefined ratio of the tensile to compressive Young's modulus of each real material. However, the main building materials in the construction industry are concrete and (structural) steel, of which each has comparable elasticity moduli either in tension as in compression and thus they are no bi-modulus materials. According to the design principles in concrete engineering, it is preferable to use financially cheap concrete for structural elements subjected to pressure loads, whereas financially expensive steel as reinforcement has to bear tensile stresses due to the low tensile strength of concrete. Thus, concrete design primarily aims at reinforcing concrete only where indispensible, i.e., where tensile stresses are present, in order to minimize the costs of the structure. It appears inaccurate to define a sufficient pseudo ratio of tensile to compressive elasticity moduli to achieve proper material separation. In addition, the existing multi-material MRM approach in Cai et al. (2016) can lead to results where a strict material separation in compressive and tensile structural members is insufficient, e.g., tension affine material is sometimes locally applied to regions that are predominantly under compressive stresses and vice versa.

Therefore, a new multiphase MRM approach will be presented that is based on gradually steering the element towards a preferable material based on the current stress state instead of switching between the different elasticity moduli. In contrast to the existing generalized multi-material MRM approach, our presented approach is tailor-made for the particular use in concrete engineering. The proposed alternative bi-material MRM approach cannot be derived directly from the existing method proposed in Cai et al. (2016). Comparable to the single-material MRM approach (Cai 2011), modification factors are defined, [see (7) and (8)], yet including in each element *both*, the compressive as well as the tensile factor $\bar{R}_-$ and $\bar{R}_+ = 1 - \bar{R}_-$ [see (9)], respectively. Hence, a compression-only (concrete) and a tension-only (structural steel) material are given in the complementary assembly of the elemental stiffness matrix stated in (12). The material models applied to approximate, for instance concrete and steel, are shown in Fig. 1.

By that, each modified element stiffness matrix $\bar{\boldsymbol{k}}_R$ is interpolated between the two modified isotropic stiffness matrices of the predefined materials in each iteration step instead of switching discretely between them

$$\begin{aligned}\bar{\boldsymbol{k}}_R(\bar{\chi},\bar{\varphi}) &= \bar{\chi}^p\left[\bar{\varphi}\;\bar{R}_-\,\bar{\boldsymbol{k}}_- + (1-\bar{\varphi})\;\bar{R}_+\,\bar{\boldsymbol{k}}_+\right]\\ &= \bar{\chi}^p\left[\bar{\varphi}\;\bar{R}_-\,\bar{\boldsymbol{k}}_- + (1-\bar{\varphi})\;(1-\bar{R}_-)\,\bar{\boldsymbol{k}}_+\right]\end{aligned} \tag{17}$$

where the phase variable $\bar{\varphi}$ steers the compressive to tensile material ratio and $\bar{\boldsymbol{k}}_-$ and $\bar{\boldsymbol{k}}_+$ denote the isotropic element stiffness matrices corresponding to the isotropic replacing materials of concrete and steel. Assembling the modified element stiffness matrices $\bar{\boldsymbol{k}}_R$ yields the modified global stiffness matrix $\boldsymbol{K}_R$. The stress state in each "hybrid" element is computed by composing the effective element elasticity matrix in a similar manner and thus interpolating linearly between the elasticity matrices for the compressive and tensile material $\bar{\mathbb{E}}_-$ and $\bar{\mathbb{E}}_+$, viz

$$\bar{\mathbb{E}} = \bar{\chi}^p\left[\bar{\varphi}\;\bar{\mathbb{E}}_- + (1-\bar{\varphi})\;\bar{\mathbb{E}}_+\right] \tag{18}$$

which corresponds to a Voigt bound of the mixture energy of the tension affine and compression affine material. In contrast, the existing multi-material MRM approach in Cai et al. (2016) switches between the elasticity matrices of the two predefined replacing materials for each real material. Of course, other mixture rules might be applied,

such as the effective elastic constants according to Reuss or Mori-Tanaka (Mori and Tanaka 1973). However, the Voigt mixture is in accordance to the tension/compression anisotropy enhancement in (17).

Again, it is important to note that for linear FE analysis, i.e., calculation of deformations, strains, and stresses, the bi-linear material behavior shown in Fig. 1 is replaced by two linear elastic, isotropic materials assembling each local isotropic (unmodified) stiffness matrix $\bar{\boldsymbol{k}}(\bar{\chi}, \bar{\varphi})$, cf. (12). The tension/compression anisotropy is tackled afterwards in an indirect manner by modifying the stiffness matrix according to (17). Subsequently, the sensitivities are computed using the modified element stiffnesses to update the design variables heuristically by solving a subproblem in each iteration. As Cai (2011) pointed out in the original article, in the first iteration steps the stress and strain fields of the original anisotropic and replacing isotropic materials differ strongly because most elements are under a complex stress state and mixed material elements exist. Therefore, stiffness modification of each element is momentous. As firstly material distribution evolves and structural members are arranged such that they carry predominantly one-dimensional stresses and secondly this leads to a full phase separation and adequate distribution within the design space (compression affine material in compressive stress dominating areas and likewise for tension affine material), the computational error vanishes since no more stiffness modification is performed, viz the difference between the values of structural compliance calculated with unmodified and modified stiffnesses will tend to zero. This will be demonstrated in Section 6. As a result, if an element is subjected to a stress state with predominantly uniaxial stresses, it becomes beneficial for the minimization of the objective function to steer the material distribution towards monophasic elements. Thus, the modification factors cause virtually an implicit penalization of composite elements as a consequence of their inferiority to "pure" elements. In other words, the stiffness of a composite material is usually always lower, due to the stiffness reduction of the disadvantageous material proportion, than that of monophasic elements.

In order to illuminate this strong tendency to material separation within an element, (17) is investigated in terms of the effective Young's modulus given by

$$\bar{E}_R(\bar{\chi}, \bar{\varphi}) = \bar{\chi}^p \left[\bar{\varphi}\ \bar{R}_-\ E_- + (1-\bar{\varphi})\ (1-\bar{R}_-)\ E_+\right]\ . \tag{19}$$

Mention that this illustrative effective "elemental" Young's modulus must not be confused with the effective elasticity according to (18) – whereas $\bar{\mathbb{E}}$ is used for the computation of the stresses (after $\bar{\varphi}$ has been determined), the tension/compression anisotropy enhancement follows from $\bar{\boldsymbol{k}}_R(\bar{\chi}, \bar{\varphi})$ in (17) which is supposed to be analyzed for the one-dimensional case in terms of $\bar{E}_R(\bar{\chi}, \bar{\varphi})$.

For a fixed $\bar{\chi}^p$, the resulting element stiffness $\bar{E}_R(\bar{\chi}, \bar{\varphi})$ in (19) can be plotted in the $(\bar{\varphi}, \bar{R}_-)$ space. Figure 2 shows the plot for a Young's modulus ratio of $E_+/E_- = 4$, which is a typical ratio of steel to UHPC. In the left contour plot, the color gradient corresponds to the element stiffness $\bar{E}_R(\bar{\chi}, \bar{\varphi})$, which is highlighted additionally by the isolines. Obviously, two boundary value maxima can be observed (right plot): the one representing an element fully assigned to the compressive material for $\bar{\varphi} = 1$ and $\bar{R}_- = 1$ leading to $\bar{E}_R = E_-$, and vice versa, i.e. full tensile material for $\bar{\varphi} = 0$ and $\bar{R}_- = 0$ with $\bar{E}_R = E_+$. These two single points constitute the optimal distribution, both in terms of $\bar{\chi}$ (purely one-dimensional stress) and $\bar{\varphi}$ (monophasic elements). Now, the graph can be split vertically in two sections, divided by the isoline for which $\partial \bar{E}_R / \partial \bar{\varphi} = 0$ holds (red dashed line). From this condition, the modification factor $\bar{R}_-$ is calculated as $\bar{R}_- = E_+/(E_+ + E_-)$ and hence for $E_+/E_- = 4$ it yields $\bar{R}_- = 0.8$. For a given modification factor $\bar{R}_- < E_+/(E_+ + E_-)$, it is evident that to minimize the mean compliance the most reasonable phase distribution leading to maximum element stiffness is given for $\bar{\varphi} \to 0$, hence resulting in full tensile material. On the contrary, for $\bar{R}_- > E_+/(E_+ + E_-)$ the reverse applies. Altering the predefined materials, for instance replacing UHPC with ordinary concrete exhibiting a lower Young's modulus, the threshold value for $\bar{R}_-$ increases, thus favoring the tension affine material for a broader range of stress states and vice versa. Given the assumption that, after the basic optimized design has been found through the distribution of the density χ, the fundamental stress state in an element between two iterations barely changes, a strong tendency of the phase variable is observed towards a district 0-1 distribution based on the modification factor $\bar{R}_-$. There is merely one single value, i.e. $\bar{R}_+ = E_+/(E_+ + E_-)$, for which all yielding points are turning points, hence all values for $\bar{\varphi}$ result in the same element stiffness and thus a 0-1 distribution is not given. Except this, from a numerical point of view, highly unlikely event, a rigorous material separation is indispensable for the minimization of the objective function. In reference to the discussion of an additional penalization exponent for the phase variable in Section 3.1, besides the lack of physical interpretation, there is indeed not even a necessity in further penalizing φ. Numerical studies underline this conclusion and will be demonstrated exemplarily in Section 6.4.

3.3 Numerical implementation

The presented approach is implemented in Matlab inspired by the pioneering work of Sigmund (2001a) and making use of the computational improvements presented in Andreassen et al. (2011). Quadrilateral 4-node elements with linear shape functions are used to discretize evenly the feasible design space Ω. The method of moving asymptotes (MMA) (Svanberg 1987), with default settings as described in (Svanberg 2007), is used to solve the minimization problem. The sensitivity analysis for the replacing isotropic material can be computed with the adjoint method, when the constraints are considered, by

$$\frac{\partial c(\bar{\boldsymbol{\chi}},\bar{\boldsymbol{\varphi}})}{\partial \bar{\chi}_e} = -p\ \bar{\chi}_e^{p-1}\ \hat{\boldsymbol{u}}_e^T \cdot \left[\bar{\varphi}_e\ \bar{\boldsymbol{k}}_- + (1-\bar{\varphi}_e)\ \bar{\boldsymbol{k}}_+\right] \cdot \hat{\boldsymbol{u}}_e, \quad (20)$$

$$\frac{\partial c(\bar{\boldsymbol{\chi}},\bar{\boldsymbol{\varphi}})}{\partial \bar{\varphi}_e} = -\bar{\chi}_e^{p}\ \hat{\boldsymbol{u}}_e^T \cdot \left[\bar{\boldsymbol{k}}_- - \bar{\boldsymbol{k}}_+\right] \cdot \hat{\boldsymbol{u}}_e\ . \quad (21)$$

For the tension/compression enhancement, the stiffness matrices and thus the sensitivities computed with the replacing isotropic material formulation are modified element-wise. The modified sensitivities applied for the subproblem then read:

$$\left.\frac{\partial c(\bar{\boldsymbol{\chi}},\bar{\boldsymbol{\varphi}})}{\partial \bar{\chi}_e}\right|_R = -p\ \bar{\chi}_e^{p-1}\ \hat{\boldsymbol{u}}_e^T \cdot \left[\bar{\varphi}_e\ \bar{R}_-\ \bar{\boldsymbol{k}}_- + (1-\bar{\varphi}_e)\ \bar{R}_+\ \bar{\boldsymbol{k}}_+\right] \cdot \hat{\boldsymbol{u}}_e, \quad (22)$$

$$\left.\frac{\partial c(\bar{\boldsymbol{\chi}},\bar{\boldsymbol{\varphi}})}{\partial \bar{\varphi}_e}\right|_R = -\bar{\chi}_e^{p}\ \hat{\boldsymbol{u}}_e^T \cdot \left[\bar{R}_-\ \bar{\boldsymbol{k}}_- - \bar{R}_+\ \bar{\boldsymbol{k}}_+\right] \cdot \hat{\boldsymbol{u}}_e\ . \quad (23)$$

For the volume constraint function formulated in (13), the sensitivity analysis simply leads to

$$\frac{\partial f(\bar{\boldsymbol{\chi}})}{\partial \bar{\chi}_e} = \Omega_e\ . \quad (24)$$

To ensure existence of solutions, and consequently mesh-independence which also implies to avoid the well-known checkerboard problem (Diaz and Sigmund 1995), additional restrictions to the optimized design have to be considered. For the method proposed in this paper, one of the most popular tools in terms of the sensitivity filter (Sigmund 1997) is implemented which modifies the derivative stated in (22). A predefined filter radius $r_{\min}$ controls the minimum structural member size and is given in terms of h, which is the element edge length. The derivatives with respect to the phase variables φ can also be modified as reported in Sigmund (2001b). However, numerical studies revealed that filtering the sensitivities of φ has no significant effect on the resulting topology (cf. Fig. 3). In transition areas between two phases fine branches can still appear causing mesh dependency. Applying a filter on the phase variables can remove these fine branches and ensure a smooth transition. Thus, filtering techniques could be used to apply manufacturing constraints for the phase. However, this topic is beyond the scope of this publication. Furthermore, the results presented in Section 6.4 demonstrate that no additional constraint has to be employed in order to avoid composite elements, i.e., elements with mixed material distribution. Hence, sensitivity filtering with respect to the phase variables is not adopted hereafter.

Special attention is required regarding the stop criterion of the iterative optimization procedure. In the 99-line code (Sigmund 2001a) as well as in the 88-line code (Andreassen et al. 2011), an absolute convergence criterion

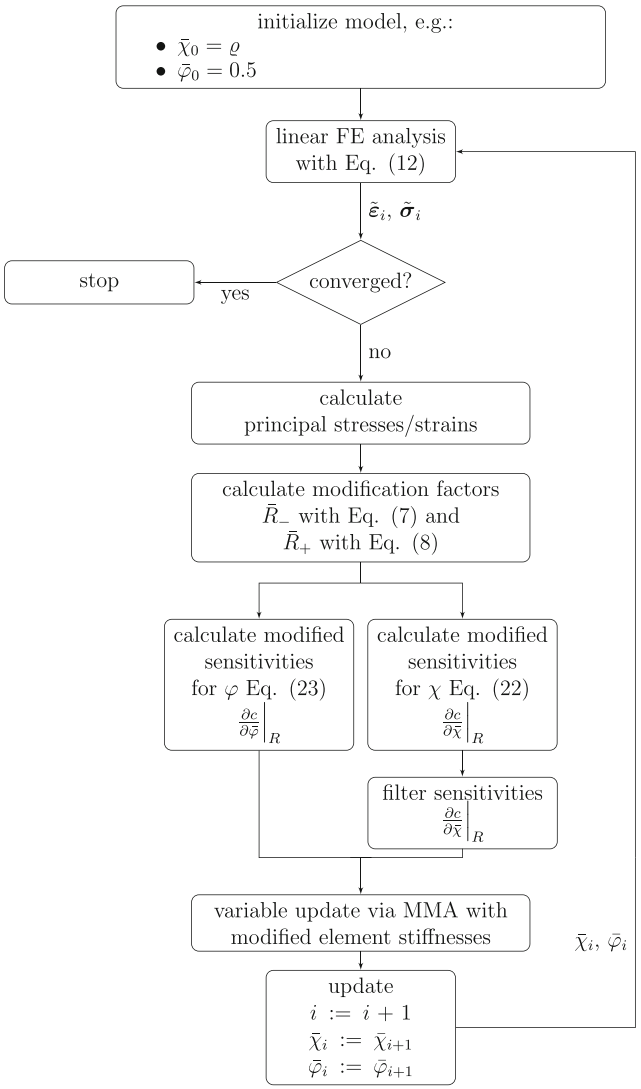

Fig. 4 Flowchart for the extended MRM

is implemented based on the maximum change of an element density between two iterations, i.e.

$$\max \Delta\chi = \max_e \left| \bar{\chi}_e^{i-1} - \bar{\chi}_e^{i} \right| \leq 10^{-2} \,, \tag{25}$$

where i is the current iteration step. An alternative convergence criterion referring to the relative change of the objective function, i.e., the mean structural compliance c, between two iteration steps can be formulated as

$$\Delta c_{\text{rel}} = \left| \frac{c^{i-1} - c^{i}}{c^{i}} \right| \leq \text{ctol} \,. \tag{26}$$

It has been observed that the fundamental layout of the optimized structure is found in the first, often relatively few iterations. By imposing an absolute stop criterion like that given in (25), the possibility of an extended search procedure arises in which usually only marginal improvements can be obtained, if at all. Since MRM is a heuristic approach in which the element stiffness and thus the sensitivities are modified in each iteration, a few element densities can oscillate between iterations particularly in elements exhibiting a multi-dimensional stress state. Thus, it is more promising to adopt a relative criterion like that proposed in (26). However, special attention has to be paid regarding the convergence limit ctol. If ctol is chosen too large the probability of a premature finish of the search process arises. On the contrary, a very small value could lead to a considerable great number of iterations. Numerous numerical studies exhibit that ctol $= 10^{-6}$ is an adequate stop limit. Nevertheless, the total iteration number should be limited to avoid potentially extensive iterations in the optimization process.

A flowchart of the presented MRM approach is given in Fig. 4. After the stresses and strains are computed by a linear FE analysis for the replacing isotropic material, the modification factors $\bar{R}_-$ and $\bar{R}_+$ are determined by (7) and (8). The modified derivatives are thereby computed with (22), (23) and (24) to update the design variables via MMA, hence incorporating tension/compression anisotropy in the linear FE analysis heuristically. The FE analysis of the subsequent iteration step is then carried out again with the global stiffness matrix assembled from the unmodified element stiffness matrices given by (12) but which are now composed by the updated design variables. The previously modified stiffness is replaced by the unaltered (isotropic material behavior) before each new iteration, hence the name of the approach.

4 Thermodynamic topology optimization

4.1 Preliminaries

The thermodynamic topology optimization was derived in a series of papers of which just the basics are recalled for convenience. Further details can be found in the original publications (Junker and Hackl 2015, 2016; Jantos et al. 2016, 2018b). The fundamental idea of the TDO is the usage of thermodynamic principles known from material modeling. Hereto, Hamilton's principle has been proven to be beneficial. In contrast to the procedure for tension/compression anisotropy enhancement of the MRM in which a modification of the stiffness matrix for the optimization was performed, it will be shown that the fundamental idea in Section 2 is applicable also by an energetic penalization. To this end, the original model is extended by a second functional including the penalization potential $\mathcal{P}$, which is specified in Section 4.2, to address the tension/compression anisotropy. This yields

$$\begin{aligned} \delta\mathcal{G} + \int_\Omega \frac{\partial \mathcal{D}_\chi}{\partial \dot{\chi}} \delta\chi \, \mathrm{d}V + \delta\mathcal{C}_\chi + \delta\mathcal{R} &= 0 \quad \forall\, \delta\boldsymbol{u},\ \delta\chi \\ \delta\mathcal{P} + \int_\Omega \frac{\partial \mathcal{D}_\varphi}{\partial \dot{\varphi}} \delta\varphi \, \mathrm{d}V + \delta\mathcal{C}_\varphi &= 0 \quad \forall\, \delta\varphi \end{aligned} \tag{27}$$

as stationarity condition(s) where $\mathcal{G}$ is the Gibbs energy with the displacements $\boldsymbol{u}$. $\mathcal{D}_\chi$ and $\mathcal{D}_\varphi$ are the dissipation functions with the internal variables $\chi(\boldsymbol{x})$ and $\varphi(\boldsymbol{x})$, which equal the design variables in the context of optimization. The two design variables for the topology optimization with tension/compression anisotropy are defined as already done for the MRM: the local material's density $\chi \in [\chi_{\min}, 1]$ and the tension/compression phase $\varphi \in [0, 1]$. The functionals $\mathcal{C}_\chi$ and $\mathcal{C}_\varphi$ account the problem-specific constraints for χ and φ, respectively, and the functional $\mathcal{R}$ refers to a regularization. The Gâteaux derivative, indicated by a prefixed δ, refers to a "total derivative" with respect to all variables that are present in the respective model approach, i.e. the displacement field $\boldsymbol{u}$ and the design (or internal) variables χ and φ.

The problem is separated in the two stationarity conditions (27) to decouple the phase evolution imposed by $\mathcal{P}$ from the mechanical problem represented by $\mathcal{G}$. The inclusion of the phase variable to the mechanical problem would yield an evolution towards the stiffer phase, which is physically reasonable but not intended for the present model. Instead, we want to provide the evolution of the material phase based purely on the local distinction between tension and compression, which is a rather unphysical

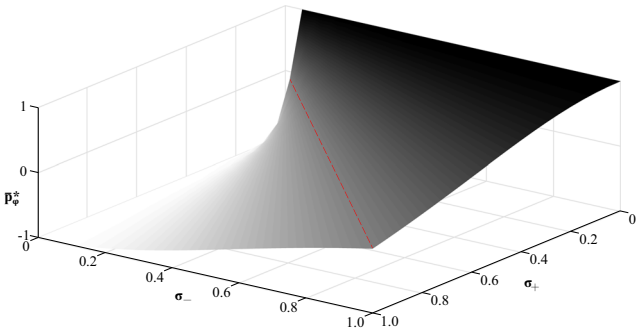

Fig. 5 Driving forces $\bar{p}_{\varphi^*}$ for the phase variable φ with respect to the principal stresses $\sigma_i = \{\sigma_+, \sigma_-\}$. The red dashed line denotes the threshold $\bar{p}_{\varphi^*} = 0$

property for linear elastic materials. Thus, we decouple the mechanically/physically motivated topology optimization from the economically motivated phase distribution.

The Gibbs $\mathcal{G}$ energy for solid mechanics can be defined as

$$\mathcal{G} = \int_\Omega \Psi \, \mathrm{d}V - \int_\Omega \boldsymbol{f} \cdot \boldsymbol{u} \, \mathrm{d}V - \int_{\partial\Omega} \boldsymbol{t} \cdot \boldsymbol{u} \, \mathrm{d}A \tag{28}$$

where $\boldsymbol{f}$ are the body forces and $\boldsymbol{t}$ are the given external tractions that act on the boundary $\partial\Omega$. The Helmholtz free energy Ψ for a linear elastic material reads

$$\Psi = \frac{1}{2}\boldsymbol{\sigma} : [\mathbb{E}(\chi, \varphi)]^{-1} : \boldsymbol{\sigma} \tag{29}$$

where $\boldsymbol{\sigma}$ denotes the stresses and $\mathbb{E}(\chi, \varphi)$ the spatially distributed material stiffness defined by the design variables $\chi(\boldsymbol{x})$ and $\varphi(\boldsymbol{x})$. The definition of the Helmholtz free energy with respect to stresses and material compliance yields a model which minimizes the structural compliance (i.e., increases the stiffness). The definition with respect to strains and material stiffness would yield a model which minimizes the structural stiffness as in mechanical damage modeling models, e.g., Junker et al. (2017).

The material stiffness is defined as

$$\mathbb{E}(\chi, \varphi) = \chi^p \, [\varphi \, \mathbb{E}_-^{-1} + (1 - \varphi) \, \mathbb{E}_+^{-1}]^{-1} \tag{30}$$

which follows from relaxation, cf. Junker (2014), and constitutes a lower Reuss bound. This procedure is in agreement to the previous approaches to TDO but differs from the one in MRM where a Voigt bound is used. However, as will be demonstrated by the numerical results, almost no intermediate phases $\varphi \in]0, 1[$ are present for which both energy bounds yield the very same value.

For numerical reasons, the material stiffness must not be zero, which is accounted for by the small parameter $0 < \chi_{\min} \ll 1$. As for the MRM, the penalization exponent $p > 1$ known from SIMP approaches penalizes intermediate densities $\chi \in]\chi_{\min}, 1[$. The phase φ does not need additional penalization, because the tension/compression penalization, which is introduced later by the functional $\mathcal{P}$, removes intermediate phases $\varphi \in [0, 1]$. It bears emphasis that the same effective elasticity tensor $\mathbb{E}(\chi, \varphi)$ in (30) is later used both for the construction of the finite element stiffness matrix and the update scheme for the design variables which stands in contrast to the MRM, cf. Section 3.2.

The dissipation functions $\mathcal{D}_\chi$ and $\mathcal{D}_\varphi$ influence the form of the later evolution equations which are used as an update scheme for the design variables. A usual approach for viscous evolution is applied by choosing

$$\mathcal{D}_\chi = \frac{1}{2}\,\eta_\chi\,\dot{\chi}^2 \qquad \text{and} \qquad \mathcal{D}_\varphi := \frac{1}{2}\,\eta_\varphi\,\dot{\varphi}^2 \tag{31}$$

with the viscosities $\eta_\chi > 0$ and $\eta_\varphi > 0$. Although the viscosities may have a physical meaning, they are primarily used as numerical damping parameters for the iterative update of the design variables (Jantos et al. 2016, 2018a).

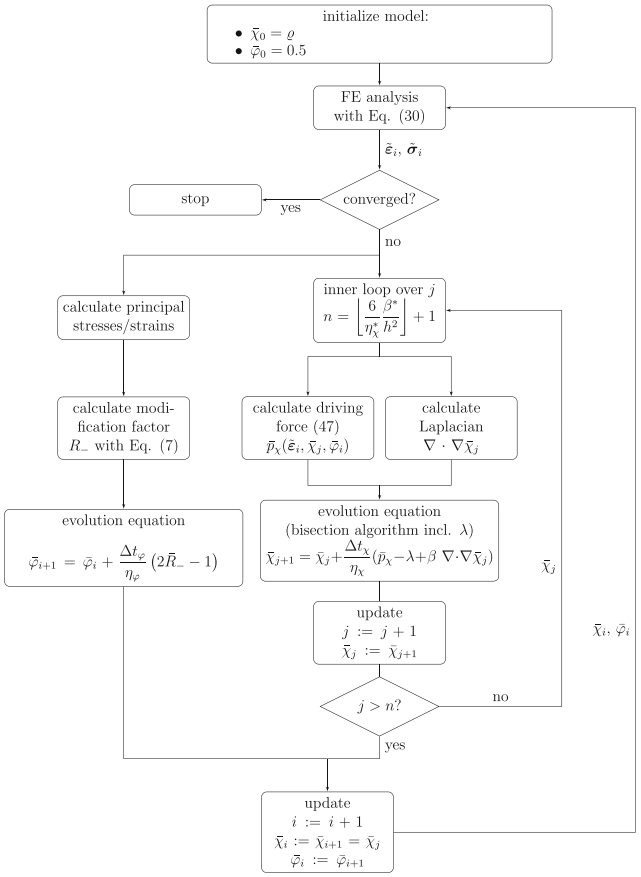

Fig. 6 Flowchart for the TDO

The functional $\mathcal{C}$ accounts the problem specific constraints

$$\varphi \in [0,1] \quad \forall \quad \boldsymbol{x} \in \Omega \tag{32}$$

$$\chi \in [\chi_{\min}, 1] \quad \forall \quad \boldsymbol{x} \in \Omega \tag{33}$$

$$\int_\Omega \chi \, \mathrm{d}V - \varrho\Omega \quad = 0 \tag{34}$$

which are identical as given for the MRM, cf. (13). Thus, the constraint functionals are defined as

$$\begin{aligned} \mathcal{C}_\chi &:= \int_\Omega \gamma_\chi \, \chi \, \mathrm{d}V + \lambda \left(\int_\Omega \chi \, \mathrm{d}V - \varrho\Omega \right) \quad \text{and} \\ \mathcal{C}_\varphi &:= \int_\Omega \gamma_\varphi \, \varphi \, \mathrm{d}V \end{aligned} \tag{35}$$

including the Lagrange multiplier λ and the Kuhn-Tucker parameters

$$\gamma_\varphi = \begin{cases} \bar{\gamma}_\varphi & : \dot{\varphi} > 0 \ \wedge \ \varphi = 1 \\ -\bar{\gamma}_\varphi & : \dot{\varphi} < 0 \ \wedge \ \varphi = 0 \\ 0 & : \quad \text{else} \end{cases} \tag{36}$$

and

$$\gamma_\chi = \begin{cases} \bar{\gamma}_\chi & : \quad \dot{\chi} > 0 \ \wedge \ \chi = 1 \\ -\bar{\gamma}_\chi & : \dot{\chi} < 0 \ \wedge \ \chi = \chi_{\min} \\ 0 & : \quad \text{else} \end{cases} . \tag{37}$$

It is well-known, that the SIMP approach for $p > 1$ yields a non-convex and mathematically ill-posed problem resulting in checkerboarding and mesh-dependent results (Sigmund and Petersson 1998; Stolpe and Svanberg 2001; Rozvany 2009). The MRM tackles the problem employing filter techniques, cf. Section 3.3. In contrast to this strategy, the fundamental problem statement for the TDO is regularized by a gradient penalization. To this end, this issue is accounted by applying a Tikhonov regularization (Engl et al. 1989; Wang and Zhou 2004; Yamada et al. 2010) for the density χ introducing the functional $\mathcal{R}$ as

$$\mathcal{R} := \int_\Omega \frac{1}{2} \beta |\nabla \chi|^2 \, \mathrm{d}V \tag{38}$$

with the nabla operator $\nabla = \partial / \partial \boldsymbol{x}$ and the numerical regularization parameter β, which can be used to control the minimum structural member size similar to filter radii of classical filtering techniques. This regularization strategy is well-known in gradient-enhanced damage modeling (De Borst and Mühlhaus 1992; Peerlings et al. 1996). Herein, the regularization parameter β corresponds to the crack width which in turn can be associated with the minimum member size in topology optimization. Further elaboration and details are given in Jantos et al. (2018a), Junker et al. (2019).

4.2 Tension/compression anisotropy enhancement by energetic penalization

In contrast to the direct modification of the stiffness matrix in the MRM, cf. Section 3.2, the fundamental idea for tension/compression anisotropy enhancement as presented in Section 2 is included into the TDO by energetic penalization. The modification factors R_- and R_+ according to (7) and (8) serve as energetic measure for a compression affine or tension affine state. Hence, the penalization functional $\mathcal{P}$ is defined by

$$\mathcal{P} = \int_\Omega \left[\varphi \, R_+ + (1 - \varphi) \, R_- \right] \mathrm{d}V \, . \tag{39}$$

Mention that for a purely tensile stress state it holds $R_- = 0$, $R_+ > 0$, and the phase variable evolves towards the tensile affine material $\varphi \to 0$. For a purely compressive state $R_+ = 0$, $R_- > 0$, and $\varphi \to 1$ holds. For both cases it holds $\mathcal{P} = 0$ and no penalization is active, i.e., the energy is at a minimum. Because the phase variable φ is linear in $\mathcal{P}$, no regularization is required for the very same. Nevertheless, regularization and/or filtering techniques could be applied to apply manufacturing constraints. However, this is beyond the scope of this work, which focuses on the overall topology design.

Collecting all functionals, the Gâteaux derivative with respect to the unknown variables given in (27) can now be evaluated. The unknown variables of the problem are the displacement field $\boldsymbol{u}$ and the design variables χ and φ. The variation with respect to $\boldsymbol{u}$ yields

$$\delta_{\boldsymbol{u}} \mathcal{G} = 0 \qquad \forall \, \delta \boldsymbol{u} \tag{40}$$

with the balance of linear momentum

$$\delta_{\boldsymbol{u}} \mathcal{G} = \int_\Omega \boldsymbol{\varepsilon} : \mathbb{E}(\chi, \varphi) : \delta \boldsymbol{\varepsilon} \, \mathrm{d}V - \int_\Omega \boldsymbol{f} \cdot \delta \boldsymbol{u} \, \mathrm{d}V - \int_{\partial\Omega} \boldsymbol{t} \cdot \delta \boldsymbol{u} \, \mathrm{d}A \tag{41}$$

where Hooke's law $\boldsymbol{\sigma} = \mathbb{E}(\chi, \varphi) : \boldsymbol{\varepsilon}$ has been inserted.

The stationarity conditions for the design variables result in partial differential equations (PDEs) which can be used as an update scheme for the χ and φ, cf. Junker and Hackl (2015, 2016), Jantos et al. (2016, 2018b). The variations with respect to the density χ yield

$$0 = \frac{\partial \Psi}{\partial \chi} + \eta_\chi \dot{\chi} + \lambda + \gamma_\chi - \beta \, \nabla \cdot \nabla \chi \quad \forall \, \boldsymbol{x} \in \Omega \tag{42}$$

$$0 = \beta \, \nabla \chi \cdot \boldsymbol{n} \quad \forall \, \boldsymbol{x} \in \partial\Omega \tag{43}$$

where $\delta\mathcal{R}$ is integrated by parts with the outward pointing normal vector $\boldsymbol{n}$ on the boundary $\partial\Omega$. The variation with respect to the phase variable φ yields

$$0 = \eta_\varphi \dot{\varphi} + \gamma_\varphi + \left[R_+ - R_-\right] \quad \forall\, \boldsymbol{x} \in \Omega \tag{44}$$

The three equations (41), (42) and (44) form a closed system for the unknowns $\boldsymbol{u}$, χ and φ, with the boundary condition (43), and can be solved numerically.

4.3 Numerical implementation

The structural analysis is carried out within a FE environment in which the displacements $\boldsymbol{u}$ are the only unknowns. The notations regarding the discretization introduced in Section 3.1 are used: $\hat{(\cdot)}$ denotes quantities discretized at the nodes of the FE mesh, $\tilde{(\cdot)}$ denotes quantities discretized at the integration (Gauß) points, and $\bar{(\cdot)}$ denotes element-wise constant quantities. Higher order tensors are given in their respective Voigt notation. The balance of linear momentum given in (41) is solved with a classical FE approach with linear shape functions. The operator matrix $\boldsymbol{b}$ is defined by $\hat{\boldsymbol{u}} = \boldsymbol{b} \cdot \tilde{\boldsymbol{\varepsilon}}$ which yields the element stiffness matrix

$$\bar{\boldsymbol{k}} = \int_{\Omega_e} \boldsymbol{b}^{\mathrm{T}} \cdot \mathbb{E}(\bar{\chi}, \bar{\varphi}) \cdot \boldsymbol{b} \, \mathrm{d}V \tag{45}$$

with the element-wise discretized design variables $\bar{\chi}$ and $\bar{\varphi}$.

Using the given discretization, (42) can be transformed to

$$\dot{\bar{\chi}} = \frac{1}{\eta_\chi} \left(\bar{p}_\chi - \lambda + \beta \, \nabla \cdot \nabla \bar{\chi} \right) \tag{46}$$

with the element-wise constant mechanical driving force $\bar{p}_\chi$

$$\begin{aligned} \bar{p}_\chi &= \frac{1}{\Omega_e} \int_{\Omega_e} -\frac{\partial \Psi}{\partial \bar{\chi}} \, \mathrm{d}V \\ &= \frac{1}{2\Omega_e} \int_{\Omega_e} \tilde{\boldsymbol{\varepsilon}} \cdot p \, \bar{\chi}^{\,p-1} [\varphi \, \mathbb{E}_-^{-1} + (1-\varphi) \, \mathbb{E}_+^{-1}]^{-1} \cdot \tilde{\boldsymbol{\varepsilon}} \, \mathrm{d}V \,. \end{aligned} \tag{47}$$

The driving force serves the same purpose as the sensitivities (Jantos et al. 2018b). The Laplacian is calculated via the finite difference scheme

$$\nabla \cdot \nabla \bar{\chi}|_{\bar{\boldsymbol{x}}} \approx \sum_{i=1}^{2} \frac{\bar{\chi}(\bar{\boldsymbol{x}} + h \, \boldsymbol{e}_i) - 2 \, \bar{\chi}(\bar{\boldsymbol{x}}) + \bar{\chi}(\bar{\boldsymbol{x}} - h \, \boldsymbol{e}_i)}{h^2} \tag{48}$$

where h is the distance between the midpoints of two neighboring elements or the length of the element edges. Applications for the Laplacian on unstructured quadrilateral (hexahedral) meshes are given in Jantos et al. (2018a). The element-wise discretization of (44) yields

$$\dot{\bar{\varphi}} = \frac{\bar{R}_- - \bar{R}_+}{\eta_\varphi} \overset{(9)}{=} \frac{2\bar{R}_- - 1}{\eta_\varphi} \tag{49}$$

with

$$\bar{R}_- = \frac{1}{\Omega_e} \int_{\Omega_e} R_- \, \mathrm{d}V \,. \tag{50}$$

The phase transformation is based solely on the spectral decomposition of the elastic energy given by $\bar{R}_-$ and $\bar{R}_+$. For $\bar{R}_- > \bar{R}_+$, $\dot{\bar{\varphi}} > 0$ and the compression affine material indicated by $\varphi \to 1$ will be established, whereas the contrary applies for $\bar{R}_- < \bar{R}_+$. The mixed bi-axial (two-dimensional) case for principal stresses given by $\sigma_i = \{\sigma_+, \sigma_-\}$ with $\sigma_+ > 0$ and $\sigma_- < 0$ is illustrated in Fig. 5.

The Kuhn-Tucker parameters γ_χ and γ_φ can be replaced by simple if-conditions within the numerical solution to grant the interval boundaries $\chi \in [\chi_{\min}, 1]$ and $\varphi \in [0, 1]$ and are omitted in the following. The viscosity related to the numerical damping η_χ and the regularization parameter β for the density field are

$$\beta = \beta^* \, p_w \tag{51}$$

$$\eta = \eta_\chi^* \, p_w \tag{52}$$

with

$$p_w = \frac{\int_\Omega g(\bar{\chi}) \, \bar{p}_\chi \, \mathrm{d}V}{\int_\Omega g(\bar{\chi}) \, \mathrm{d}V} \tag{53}$$

including

$$g(\chi) = (\chi - \chi_{\min})(1 - \chi) \quad \forall\, \chi \in [\chi_{\min}, 1] \tag{54}$$

The parameters related to the viscosity η_χ^* and the viscosity η_φ are defined as constant and problem independent with $\eta_\chi^* = 15.0$ and $\eta_\varphi = 1.0$, respectively. The parameter related to the regularization β^* is associated with the internal length of the microstructure of the problem (De Borst and Mühlhaus 1992; Peerlings et al. 1996) and can be used to control the minimum structure member size: the mimimum member size scales with $\sqrt{\beta^*}$ (Jantos et al. 2018a). Values $\beta^* \geq 2h^2$ are recommended to suppress checkerboarding and grant mesh-independent results.

Table 1 Comparison of methodology between MRM and TDO

	MRM	TDO
FEM	Linear elastic; linear shape functions	
Interpolation	SIMP (power-law) for χ	
	Voigt bound for φ	Reuss bound for φ
Material separation	Modification of element stiffness	Energetic penalization
Regularization	χ: sensitivity filter with $r_{\min}$	χ: gradient penalization with β^*
	no regularization for φ	
Optimization solver	MMA	Evolution equation given as ODE/PDE

The PDEs (42) and (44) are solved with an explicit time discretization $t_{i+1} = t_i + \Delta t$ yielding the update schemes

$$\bar{\chi}_{i+1} = \bar{\chi}_i + \Delta t \; \dot{\bar{\chi}}(\tilde{\boldsymbol{\varepsilon}}_i, \bar{\chi}_i, \bar{\varphi}_i) \tag{55}$$

$$\bar{\varphi}_{i+1} = \bar{\varphi}_i + \Delta t \; \dot{\bar{\varphi}}(\tilde{\boldsymbol{\varepsilon}}_i, \tilde{\boldsymbol{\sigma}}_i) \tag{56}$$

The strains $\tilde{\boldsymbol{\varepsilon}}_i$ and stresses $\tilde{\boldsymbol{\sigma}}_i = \mathbb{E}(\bar{\chi}_i, \bar{\varphi}_i) \cdot \tilde{\boldsymbol{\varepsilon}}_i$, whose spectral decomposition yields $\bar{R}_-$, are calculated via the FE analysis for each step i. The phase variable is then updated by

$$\bar{\varphi}_{i+1} = \bar{\varphi}_i + \Delta t \; \frac{2\bar{R}_- - 1}{\eta_\varphi} \tag{57}$$

The evolution equation $\dot{\bar{\chi}}$ for the density variable includes the Laplacian and is consequently discretized by a FTCS (forward time and central space) scheme which is known to be conditionally stable. A Neumann stability analysis yields

$$\frac{\eta_\chi^*}{\Delta t_\chi} \geq 6 \, \frac{\beta^*}{h^2} \tag{58}$$

To fulfill this stability condition and to keep the computational costs at a minimum, an inner solution loop over the steps j is introduced for the density variable update. Consequently, the evolution equation

$$\bar{\chi}_{j+1} = \bar{\chi}_j + \Delta t_\chi \; \dot{\bar{\chi}}(\tilde{\boldsymbol{\varepsilon}}_i, \bar{\chi}_j, \bar{\varphi}_i) \tag{59}$$

is evaluated n-times with $\Delta t_\chi = \Delta t / n$. The strains $\tilde{\boldsymbol{\varepsilon}}_i$ and the phase variable $\bar{\varphi}_i$ are held constant within the inner loop over j. The number of (minimum) inner loop steps n can be obtained from (58) as

$$n = \left\lfloor \frac{6}{\eta_\chi^*} \frac{\beta^*}{h^2} \right\rfloor + 1 \tag{60}$$

where $\lfloor \cdot \rfloor$ denotes the floor function. Thus, the two time increments are $t_{i+1} = t_i + n \; \Delta t_\chi = t_i + \Delta t$ and $t_{j+1} = t_j + \Delta t_\chi$. For simplicity, $\Delta t = 1$ is employed so that the current (dimensionless) time step t_i coincides with the current iteration step i of the FE solution.

A flowchart for the thermodynamic topology optimization with tension/compression anisotropy is given in Fig. 6. After the strains $\tilde{\boldsymbol{\varepsilon}}$ and stresses $\tilde{\boldsymbol{\sigma}}$ are obtained by a FE analysis, the design variables are updated. The Lagrange multiplier λ is determined within a bisection algorithm, similar to the evaluation of the optimality criteria method (Sigmund 2001a). The regularization is embedded within the evolution equation, and with the time-explicit discretization, no additional equation systems must be solved. The evolution of the phase $\bar{\varphi}$ can be evaluated for each element separately without any further processing. The time explicit

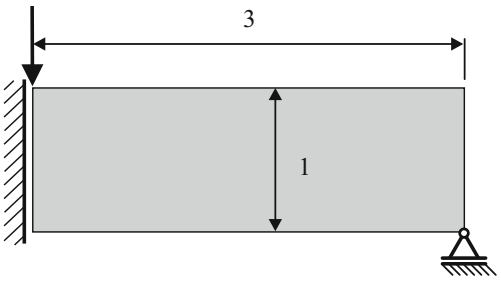

Fig. 7 Boundary conditions for the MBB beam

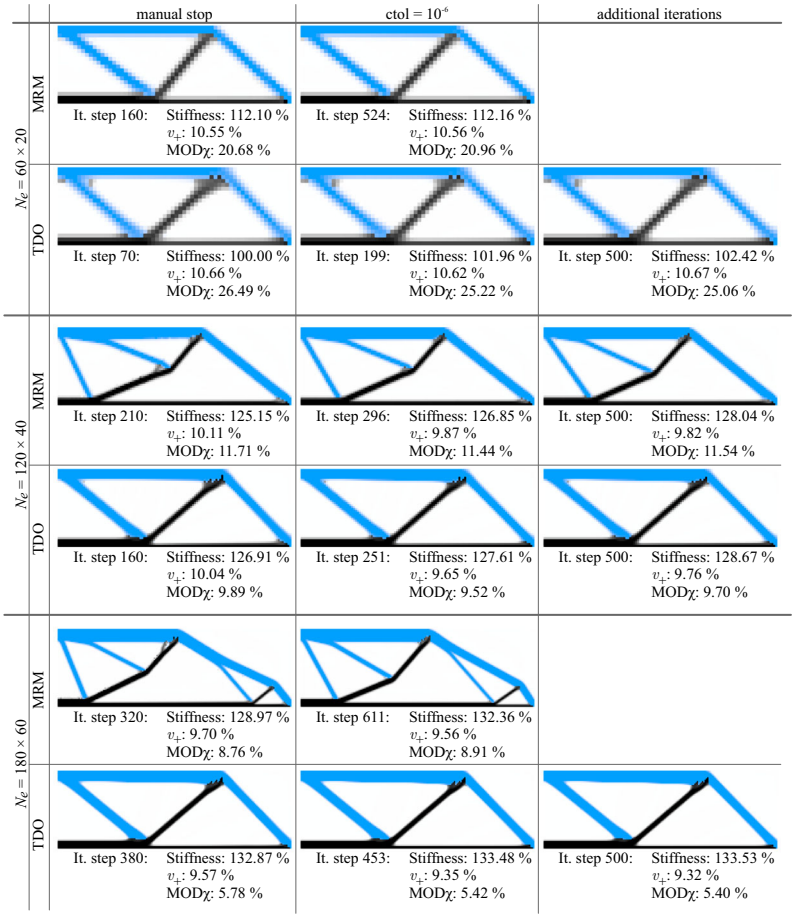

Fig. 8 Topologies obtained for the MBB beam for different meshes with $h = \{1/20,\ 1/40,\ 1/60\}$. Filter radius $r_{\min} = 1.5h$ for the MRM method and regularization parameter $\beta^* = 2.0h^2$ for the TDO method

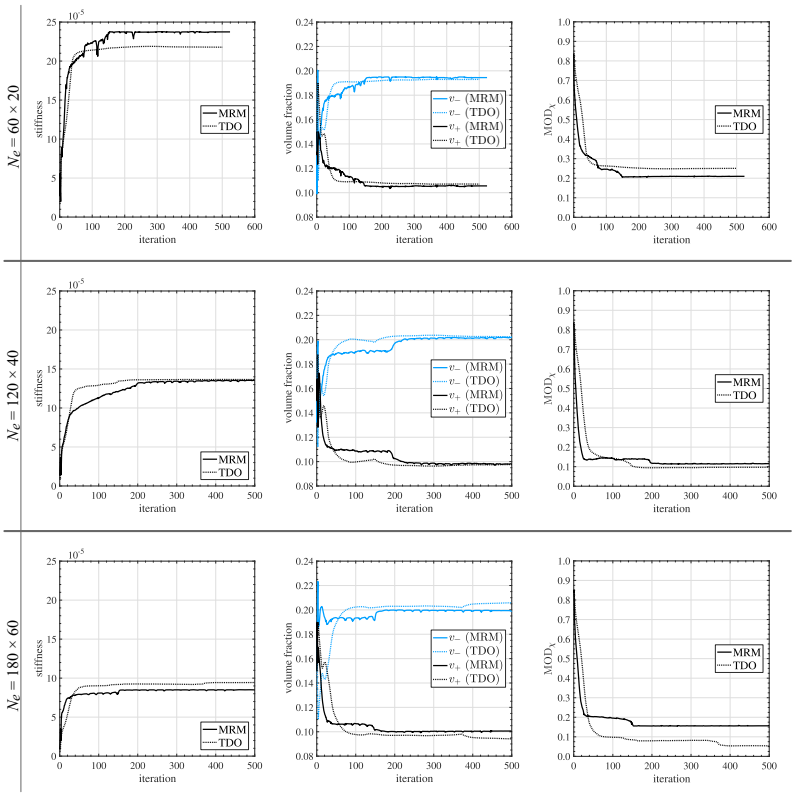

Fig. 9 Comparison of stiffness, phase volume fractions, and measure of (non-)discreteness for the MBB beam corresponding to Fig. 8. Meshes with $h = \{1/20,\ 1/40,\ 1/60\}$ and filter radius $r_{\min} = 1.5h$ for the MRM method and regularization parameter $\beta^* = 2.0h^2$ for the TDO method

updates for both internal variables $\bar{\chi}$ and $\bar{\varphi}$ are decoupled and can be solved separately.

The updated design variables are used for a new FE analysis. The process is repeated until convergence is reached. The same convergence criterion is used as for the MRM given in (26).

5 Comparison of the approaches

After applying the general idea for tension/compression anisotropy enhancement from Section 2 to two different approaches to topology optimization in Sections 3 and 4, respectively, it is convenient to make a brief comparison before analyzing actual optimization results in the next section. Table 1 contains a short comparison of the approaches.

Both methods adopt the well-established three-phase SIMP interpolation scheme. While the density variable χ is interpolated equally, the phase distribution, namely, the choice of values for φ, differs. The MRM-based approach applies a Voigt interpolation of the individual materials, which is used for the FE calculation. The stiffness matrix for the optimization is modified proportionally in dependence of the relative compression and tension parts of the elastic energy. For example, if an element consists fully of the tensile material but is in a compression dominated state, the stiffness is pushed towards zero before the design update, thus forcing the optimization algorithm to replace the disadvantageous material in order to preserve stiffness. Compressive states on tensile material are canceled out and vice versa. Hence, the approach is heuristic since different stiffness matrices are used for the FE analysis and the optimization to avoid computationally expensive nonlinear FE computations.

In contrast, TDO uses a Reuss interpolation of the individual materials. An additional functional $\mathcal{P}$ adds an energetic penalization which yields the evolution equation that is used to update the phase variable. The driving forces for the density field, which fulfill the purpose of sensitivities, are not modified, in contrast to MRM.

In conclusion, MRM can be implemented in generalized optimization algorithms such as MMA, SLP or SQP, since common sensitivity analysis with respect to φ can be carried out. For TDO, no external optimization algorithm is necessary as the Hamilton principle directly yields an ODE that leads to an evolution equation for updating the phase variable. These equations can be implemented in any FE code using the material model interface subroutine. As a consequence, a viscosity is introduced for each design variable that serves as numerical damping parameter to control the convergence behavior. In contrast, MRM is free of additionally introduced parameters apart from those of the chosen optimizer.

Though the proposed approaches diverge concerning the material update concept, they also share some commonalities. Some additional constraints have to be applied on both to ensure mesh-independent results. However, the adopted measures (filter and gradient based regularization, respectively) only need to be utilized on the density variable χ. The phase variable is not regularized within both approaches in the attempt at computing an optimized topology design although additional constraints could be applied on φ to allow for manufacturing constraints. Furthermore, no additional penalization has to be imposed on mixed phases $\varphi \in]0, 1[$ in order to ensure discrete distribution and thus material separation within elements. Both approaches make use of linear FE analysis, hence preventing sophisticated and expensive nonlinear FE analysis.

6 Numerical results

6.1 Preliminaries

The following numerical examples are obtained using uniformly distributed quadratic finite elements with bilinear shape functions. All loads are of the magnitude "1". The element edge length is denoted by h. The structural stiffness of the resulting designs is given by the inverse of the mean compliance, i.e. c^{-1}. The utilized materials are defined by their Young's moduli $E_- = 1$ for the compression affine and $E_+ = 4$ for the tension affine, respectively. The Poisson's ratio is set to $\nu_- = 0.2$ and $\nu_+ = 0.3$, respectively. The penalization exponent $p = 3$ and the lower bound $\chi_{\min} = 0.001$ are applied. The material with affinity to compression (e.g., concrete) is depicted in azure whereas the tensile material (e.g., steel) is represented by black color. For the MRM, a filter is applied on the sensitivities that is given in terms of the radius $r_{\min}$ with respect to the element length h. The regularization parameter β^* for the thermodynamic optimization (TDO) is defined analogously. For a better comparison of the results the so-called measure of discreteness with respect to the density χ is introduced (Sigmund 2007):

$$\begin{aligned} \mathrm{MOD}_\chi &= \frac{4}{\Omega}\int_\Omega (\chi - \chi_{\min})(1-\chi)\,\mathrm{d}V \\ &= \frac{4}{N_e}\sum_e^{N_e}(\bar{\chi}_e - \chi_{\min})(1-\bar{\chi}_e)\,, \end{aligned} \tag{61}$$

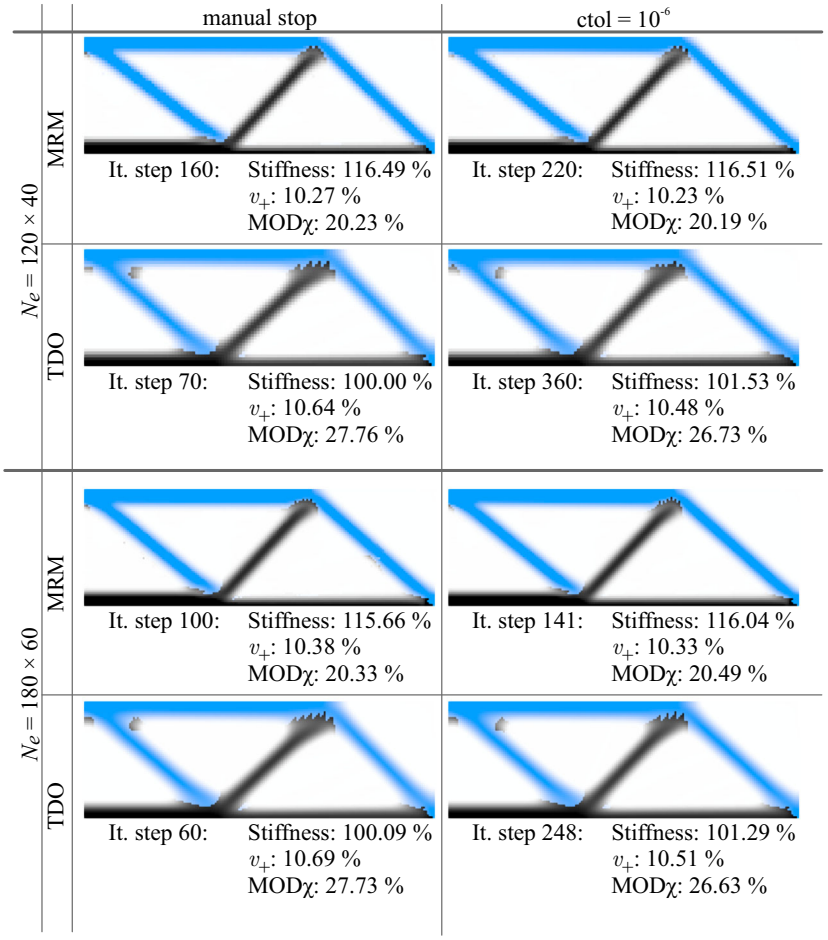

Fig. 10 Topologies obtained for the MBB beam for two different meshes with $h = \{1/40,\ 1/60\}$. Mesh-independent filter radii $r_{\min} = 3/40$ for the MRM method and the regularization parameter $\beta^* = 5 \times 10^{-3}$ for the TDO method corresponding to the coarse mesh given in Fig. 8 ($h = 1/20$) with $r_{\min} = 1.5h$ and $\beta^* = 2h^2$

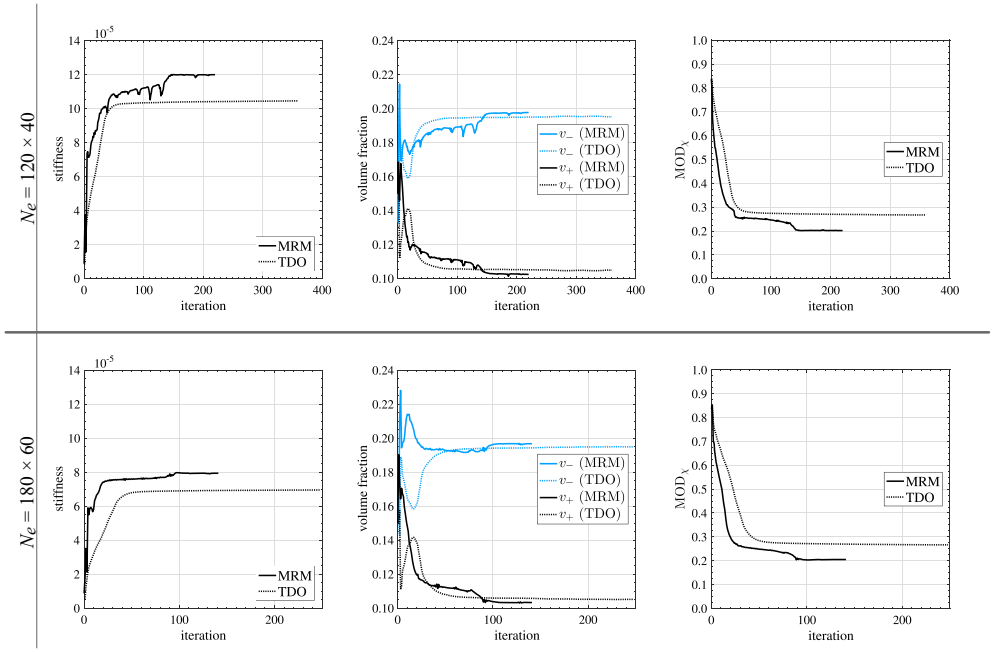

Fig. 11 Comparison of stiffness, phase volume fractions and measure of (non-)discreteness for the MBB beam corresponding to Fig. 10. Meshes with $h = \{1/40,\ 1/60\}$ and mesh-independent filterradii $r_{\min} = 3/40$ for the MRM method and the regularization parameter $\beta^* = 5 \times 10^{-3}$ for the TDO method

where $\mathrm{MOD}_\chi = 0 \mathrel{\hat{=}} 0\%$ corresponds to a fully discrete 0-1 distribution of χ and $\mathrm{MOD}_\chi = 1 \mathrel{\hat{=}} 100\%$ means that all element densities are equal to 0.5. Following this principle, a measure of discreteness can also be established for the phase variable distribution φ. It is analogously defined as

$$\begin{aligned}\mathrm{MOD}_\varphi &= 4 \int_\Omega \chi\ \varphi\ (1-\varphi)\ \mathrm{d}V \Big/ \int_\Omega \chi\ \mathrm{d}V \\ &= 4 \sum_e^{N_e} \bar{\chi}_e\ \bar{\varphi}_e\ (1-\bar{\varphi}_e) \Big/ \sum_e^{N_e} \bar{\chi}_e \quad . \end{aligned} \tag{62}$$

Here, each element phase variable is multiplied with the affiliated density in order to ensure the measure is only computed for the solid structure and not for the overall design space. The values for MOD_φ can be interpreted in the same way as for the density, i.e., a value of 0 implies that no mixed material elements exist and $\mathrm{MOD}_\varphi = 1$ that all solid elements consist of equal material proportions.

To allow for a better demonstration of the appropriate distribution of the compression affine and tension affine material, respectively, an additional measure called "Tension/Compression Error" for each element is introduced

$$\begin{aligned}\overline{\mathrm{TCE}} = \bar{\chi} \Bigg[(1-\bar{\varphi}) \left(\frac{1-\mathrm{sgn}(\bar{\sigma}_{|\max|})}{2} \right) \\ + \varphi \left(\frac{1+\mathrm{sgn}(\bar{\sigma}_{|\max|})}{2} \right) \Bigg], \end{aligned} \tag{63}$$

where $\bar{\sigma}_{|\max|}$ is the largest principal stress in terms of the absolute amount. The signum function for a plane problem formulation is defined as

$$\mathrm{sgn}(\bar{\sigma}_{|\max|}) = \begin{cases} 1 & \text{if} \quad \max\{|\sigma_i|\} \geq 0 \\ -1 & \text{else} \end{cases} . \tag{64}$$

By integration of all error values over the design space, the TCE value for the overall structure is obtained:

$$\mathrm{TCE} = \int_\Omega \overline{\mathrm{TCE}}\ \mathrm{d}V \Big/ \int_\Omega \chi\ \mathrm{d}V = \sum_e^{N_e} \overline{\mathrm{TCE}} \Big/ \sum_e^{N_e} \bar{\chi}_e\ , \tag{65}$$

where $\mathrm{TCE} = 0 \mathrel{\hat{=}} 0\%$ means that all elements predominantly under compressive stress are fully assigned with the compression affine material and vice versa for the tension affine material in tensile regions. Consequently, $\mathrm{TCE} = 1 \mathrel{\hat{=}} 100\%$ means that all elements have been fully assigned the wrong material in terms of their tension/compression affinity. A low value for the measure TCE also demonstrates that the unmodified compliance differs only slightly from the modified compliance of the subproblem for MRM.

Finally, the total volume fraction of tensile v_+ and compressive material v_- is computed by

$$v_+ := \frac{1}{\Omega} \int_\Omega \chi\ (1-\varphi)\ \mathrm{d}V\ , \qquad v_- := \frac{1}{\Omega} \int_\Omega \chi\ \varphi\ \mathrm{d}V\ , \tag{66}$$

respectively, for which $v_+ + v_- = \int_\Omega \chi\ \mathrm{d}V / \Omega \equiv \varrho$ holds true. The quantities v_+ and v_- allow for a more detailed investigation of the numerical results presented in the following.

6.2 MBB beam

Figure 7 shows the boundary conditions for the symmetrically reduced Messerschmidt-Bölkow-Blohm (MBB) beam. The optimized design is computed for three different meshes subject to a prescribed relative structural volume of $\varrho = 0.3$ by means of the proposed methods (Fig. 8). The associated values for stiffness, material volume and measure of discreteness are plotted against the iteration numbers in Fig. 9. The stiffness of each result is normalized to the smallest value given within the respective figure. In turn, for each mesh size three results per method are shown. In the first column, there are the computed structures for a manual stop of the algorithms after observing only marginal improvements between the iterations and the second column contains the results for the predefined stop criterion given by (26). Finally, in the last column the results after 500 iterations are depicted if the stop condition is met beforehand.

For the MRM based approach, the computed structures tend to more elaborated and detailed shapes as the mesh size becomes finer with $r_{\min}$ defined relative to the mesh size. The results obtained with TDO exhibit no strong dependence on mesh refinement although the regularization parameter β^* scales with the mesh size. However, a significant correlation between mesh size and stiffness is remarkable for both methods. The stiffness rises as the mesh becomes finer, whereby simultaneously the discreteness (decreasing MOD_χ) is improved. On the one hand the improvement of stiffness is affiliated with a better approximation of the mechanical model and on the other hand, which is quite more influential, with the reduction of intermediate densities $\chi \in]\chi_{\min}, 1[$ due to the declining influence of the relative filter radius (MRM) and regularization parameter (TDO), respectively. The comparative plots of Fig. 9 indicate stiffer designs

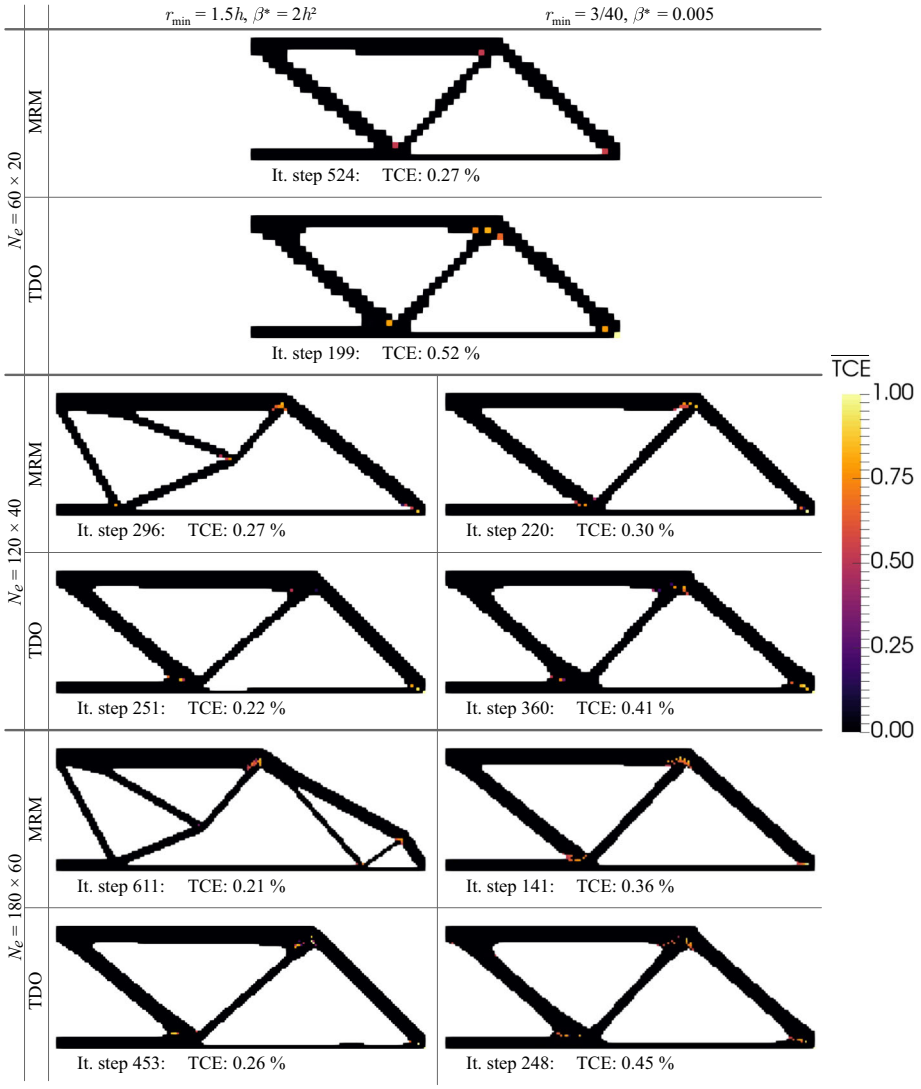

Fig. 12 $\overline{TCE}$ plots according to (63) and the overall TCE value of each structure according to (65) for the MBB results after meeting the predefined stop criterion

for TDO. By defining mesh-independent values for the regularization parameters r_{min} and β^*, as shown in Figs. 10 and 11, mesh independency can be attained for both models. As expected, the non-discreteness increases simultaneously with the degree of regularization for both methods, i.e., more blurred designs emerge.

To allow for a better comparison of the results for the MBB beam according the adequate distribution of tension affine and compression affine material, the TCE plots for the MBB beam are depicted in Fig. 12 both for MRM and TDO. The plots prove a good material distribution regarding the tension and compression affinity of the materials. The affinity is only violated for an insignificant amount of elements solely in nodes connecting the struts where a multi-dimensional stress state is present. However, the overall structural TCE value does not exceed 0.52%.

6.3 Bending problem

The classic bending problem in Fig. 13 serves as second example for the comparative numerical study. Figures 14

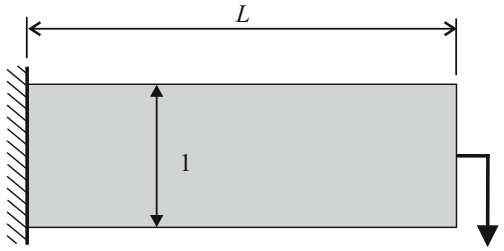

Fig. 13 Boundary conditions for the bending problem with varying length L

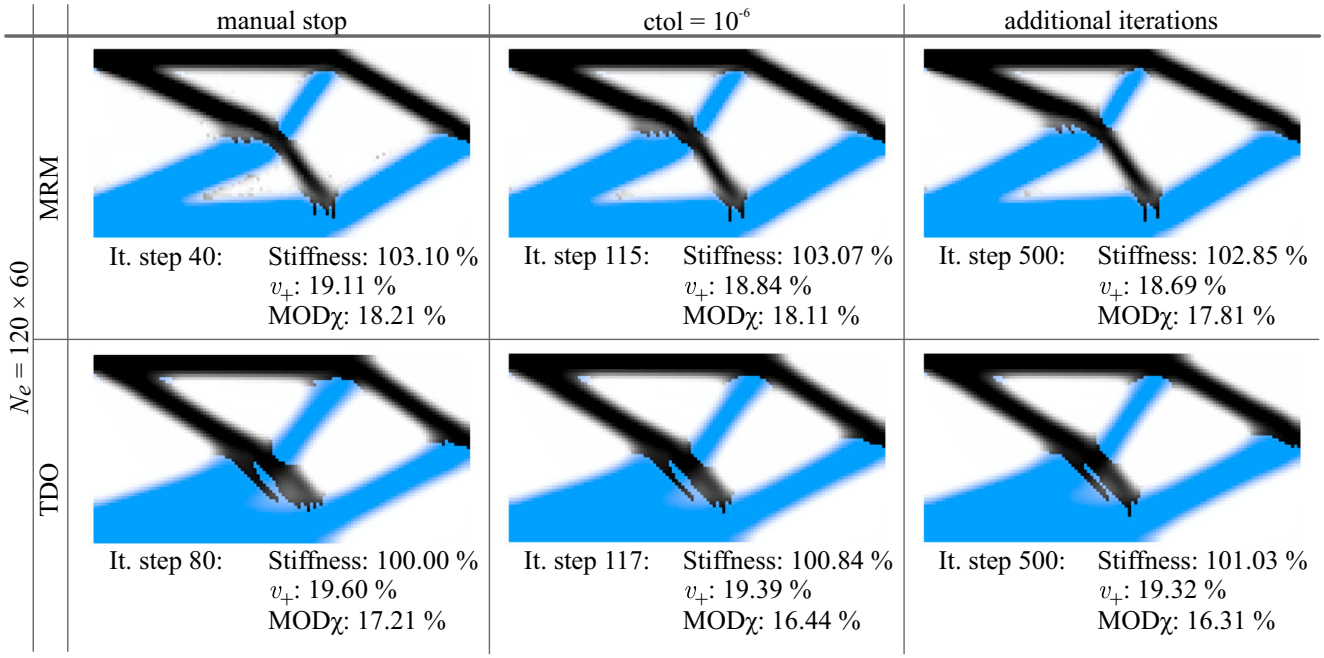

Fig. 14 Topologies obtained for the bending problem ($L = 2$) with $h = 1/60$. Filter radius $r_{\min} = 3.5h$ for the MRM method and regularization parameter $\beta^* = 8h^2$ for the TDO method

and 15 show the results for a volume fraction of $\varrho = 0.5$. As in the previous example, the obtained solutions are depicted after manual stop, satisfying the convergence criterion and for iteration number 500. Here, it is obvious that only marginal improvements can be attained for TDO by computing more iterations. In the case of MRM, the stiffness even declines slightly due to the increased amount of compression affine material used in later iteration steps, which possesses a smaller stiffness. This is reasonable, because the phase distribution in tension/compression dominated regions has a higher priority than the stiffness maximization. However, the optimized designs between MRM and TDO differ significantly, particularly in terms of the compression affine material distribution. While in MRM the bottom strut subdivides close to the clamping, in TDO the structural parts under compressive stresses are quite different from those under tensile. Although MRM employs a fewer amount of tensile material and simultaneously exhibits higher values for MOD_χ the obtained structural stiffness is throughout higher. In Fig. 16, the TCE plots and the overall TCE value are depicted for the results meeting the convergence criterion. As already observed for the MBB beam, the distribution error of materials is limited to the node areas both for MRM and TDO. However, the overall

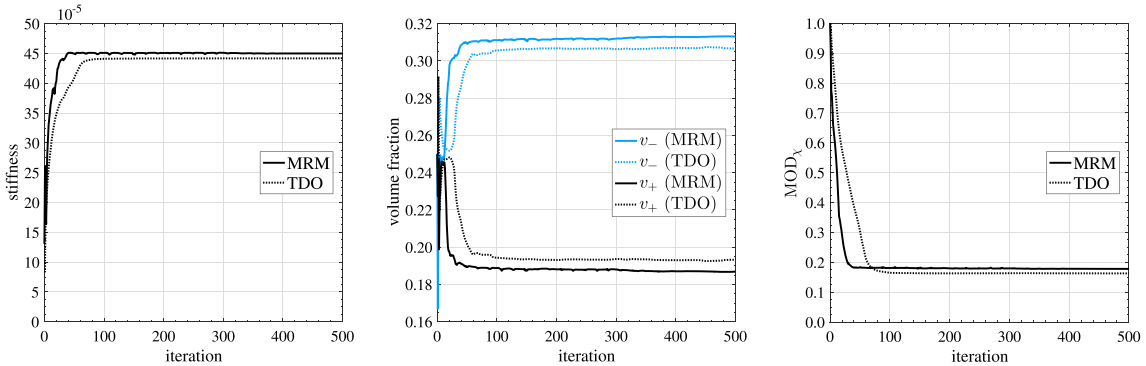

Fig. 15 Comparison of stiffness, phase volume fractions and measure of (non-)discreteness for the bending problem with $L = 2$ corresponding to Fig. 14

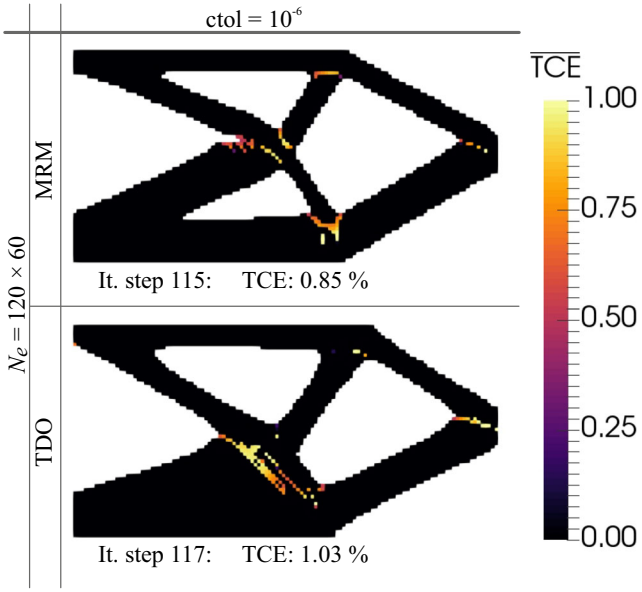

Fig. 16 $\overline{\text{TCE}}$ plots according to (63) and the overall TCE value according to (65) for the bending problem ($L = 2$) after meeting the predefined stop criterion

TCE value is very low, i.e., 0.85% for MRM and 1.03% for TDO. For a cantilever with a length of $L = 5$ as shown in Fig. 17, the TDO results are more slender and the degree of ramification is much higher compared to MRM. In fact, this contrasts to the observations made in the previous section for the MBB beam.

6.4 L-shaped cantilever

Figure 18 shows the boundary conditions for the L-shaped cantilever loaded by a single load on the top end. The aimed volume fraction is $\varrho = 0.3$ and the design space was discretized by 6 400 elements. In Figs. 19 and 20, the resulting topologies for varying filter radii and regularization parameters, respectively, are depicted. Figure 21 holds a comparative survey of the convergence history. This time the stiffness reference is of the design obtained by MRM with $r_{\min} = 3.5h$ after manual stop. All TDO results show a higher stiffness for similar acting regularization parameters compared to the filter radii in MRM, although the discreteness and the amount of tensile material is lower. It is noticeable that MRM produces designs with more spokes under tension than TDO.

Particular attention should be paid on Fig. 22 where the measure of (un-)discreteness for φ is plotted against the iteration numbers. Both, MRM and TDO, attain virtually full separation of materials within elements in the first few iterations. The MOD_φ value can be successfully reduced to 0, apart from marginal numerical fluctuations. It is

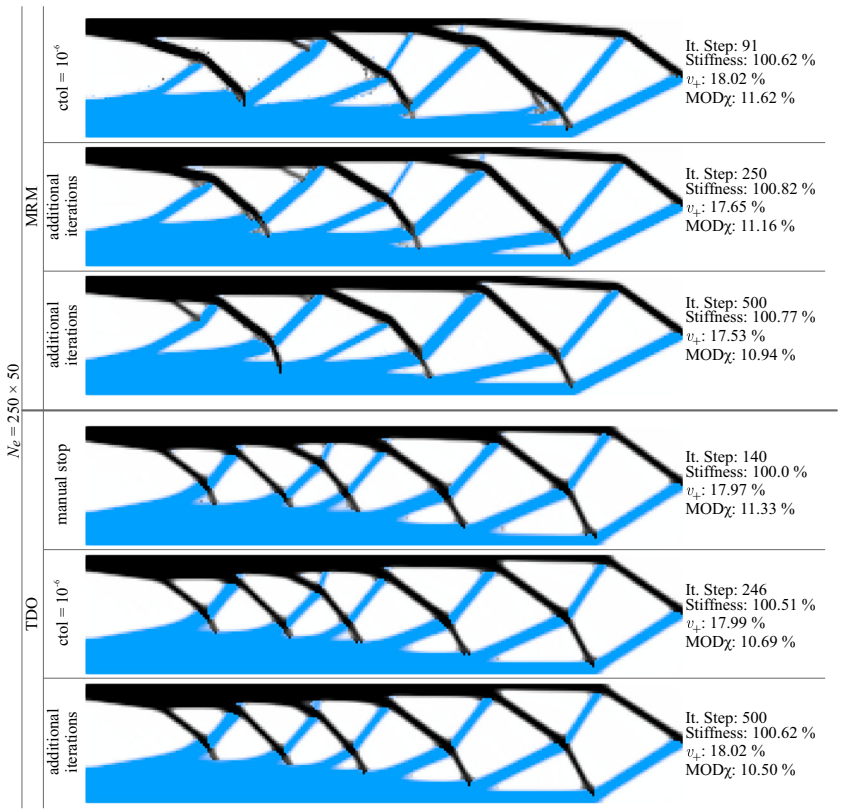

Fig. 17 Topologies obtained for the bending problem ($L = 5$) with $h = 1/60$. Filter radius $r_{\min} = 1.5h$ for the MRM method and regularization parameter $\beta^* = 2.0h^2$ for the TDO method

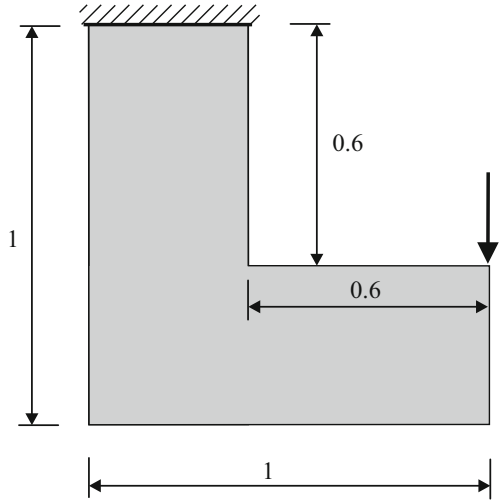

Fig. 18 Boundary conditions for the L-shaped cantilever

noticeable that discrete separation of φ is reached faster and more efficiently than that of the density variable χ. Thus, an additional penalization for mixed phases seems redundant.

Obviously, the MRM approach achieves this phase-discrete design slightly quicker throughout, whereby convergence history of TDO appears to be smoother. However, Fig. 22 is a revealing demonstration of the effectiveness of both proposed approaches in distributing materials inside the predefined design space as simultaneously distinguishing between compressive and tensile affinity.

6.5 Bridge-like problem

The symmetrically reduced bridge-like problem from Fig. 23 is computed for a volume fraction of $\varrho = 0.2$ and two different FE discretizations, one coarse with 300×100 (Fig. 24) and one fine mesh with 450×150 elements (Fig. 25). The regularization is $r_{\min} = 1.5h$ and $\beta^* = 2.0h^2$, respectively.

The results remind on arch-through bridges with suspended deck. The massive arch above the central span consists of the material with compression affinity (concrete) while it is supported from hangers consisting of the material with tension affinity (steel). The deck goes through the

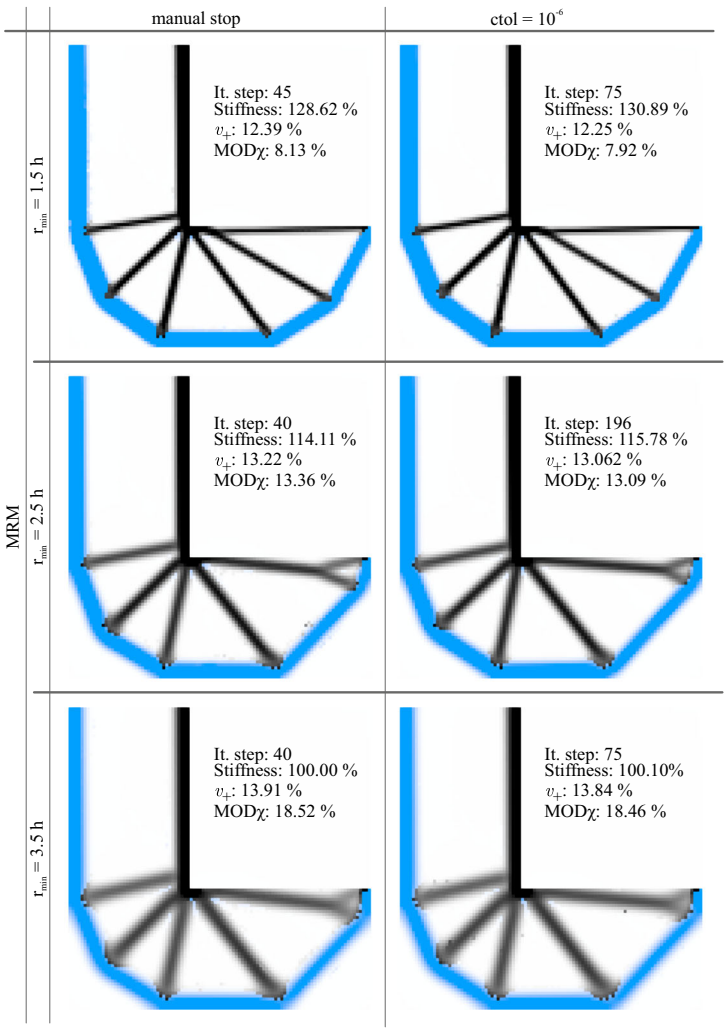

Fig. 19 Topologies obtained for the L-shaped cantilever problem with the MRM method for a mesh with $h = 1/100$ and different filterradii $r_{\min}$

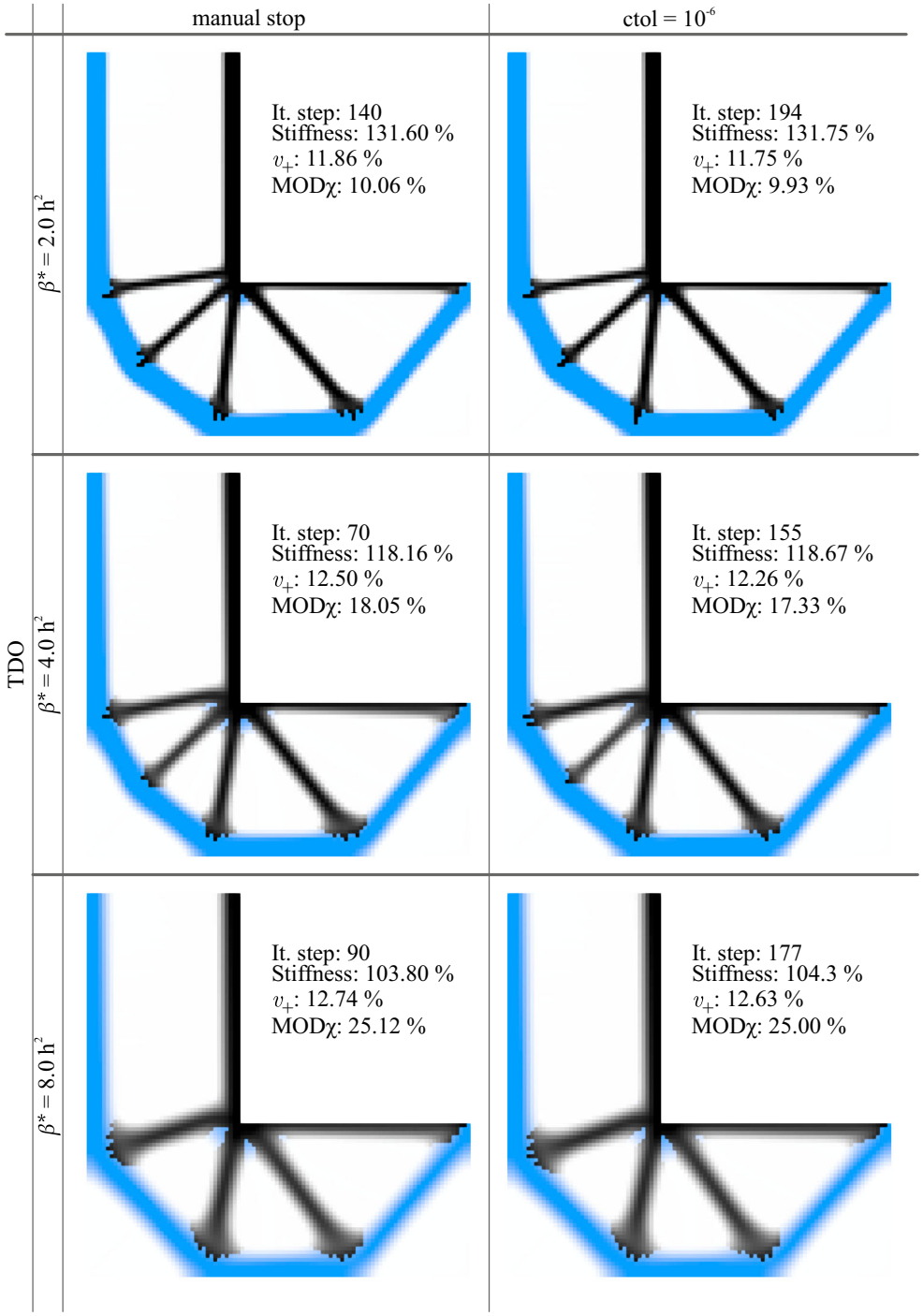

Fig. 20 Topologies obtained for the L-shaped cantilever problem with the TDO method for a mesh with $h = 1/100$ and different regularization parameters β^*

arch and the springings culminate in the supports. In turn, the cantilevering deck sections are supported by braced, fanned pylons. It is obvious that such a bridge design is well suitable for the employed construction materials, because it avoids large areas subject to bending, i.e., complex stress states. It is worth mentioning that all results limit the amount of the tensile material to approximately 3.5% what implies that the optimized structure is predominantly orientated towards a load transfer based on compression. While the TDO design converges comparatively quickly towards a convenient bridge design, MRM establishes the bridge gradually over more iteration steps. It is remarkable

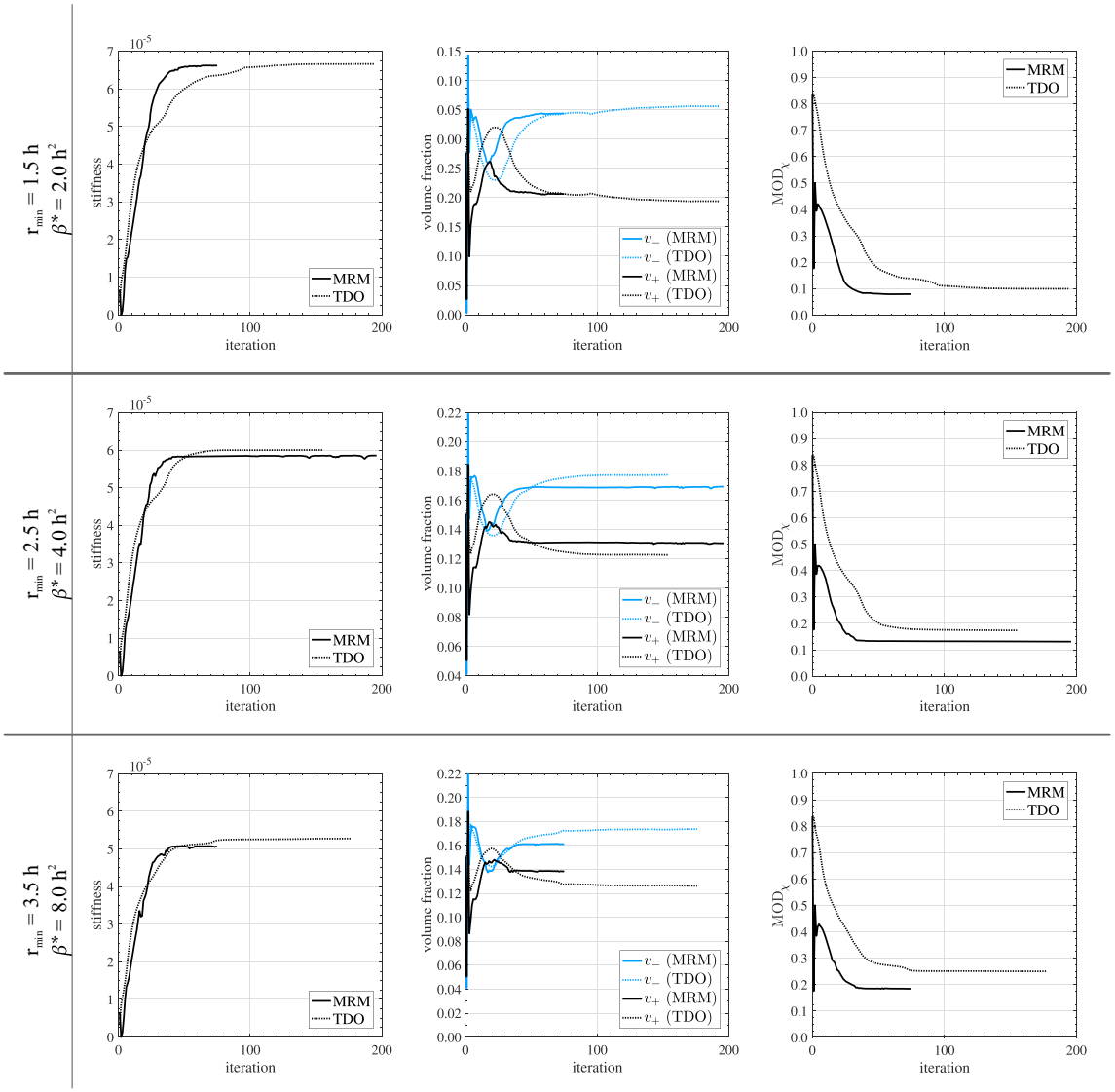

Fig. 21 Comparison of stiffness, phase volume fractions and measure of (non-)discreteness for the L-shaped cantilever problem corresponding to Figs. 19 and 20. Mesh with $h = 1/100$ and varying regularization parameters β^*

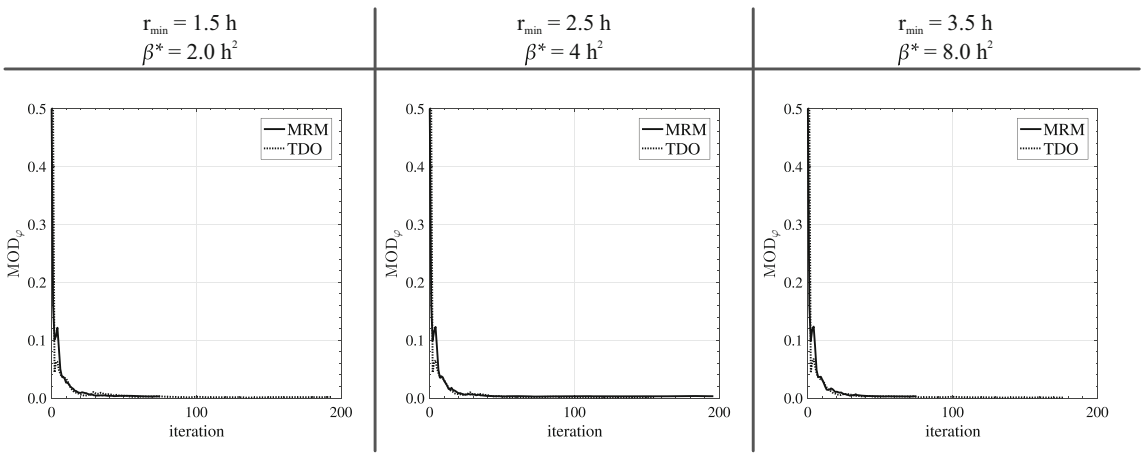

Fig. 22 Comparison of (non-)discreteness subject to the phase separation for the L-shaped cantilever problem corresponding to Figs. 19 and 20

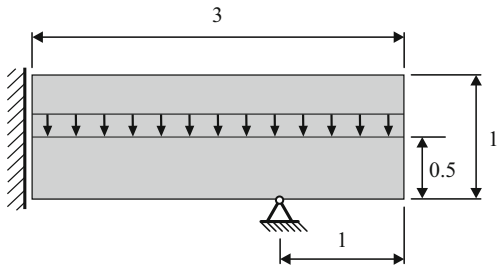

Fig. 23 Boundary conditions for the bridge-like problem

that the arch of the MRM design in both meshes is compiled gradually from two single ones. Additionally, the supporting structure above the supports evolves continuously from the bridge deck. This phenomenon known as *boundary translation problem* was already reported in Sigmund and Maute (2013) and Rojas-Labanda et al. (2017) and concerns first-order optimization methods like MMA. A better convergence for the MRM could be achieved by adjusting the parameters within the MMA algorithm. For the current examples, the default parameters according to Svanberg (2007) were applied. In contrast, TDO has only two problem independent numerical parameters to adjust, namely the viscosities η_χ and η_φ.

6.6 Multiple load cases

Optimization under multiple load cases is defined as the optimization under different loads which are not applied simultaneously on the structure (Sigmund 2001a). Multiple load cases can be taken into account by minimizing the weighted average of the compliances resulting from all

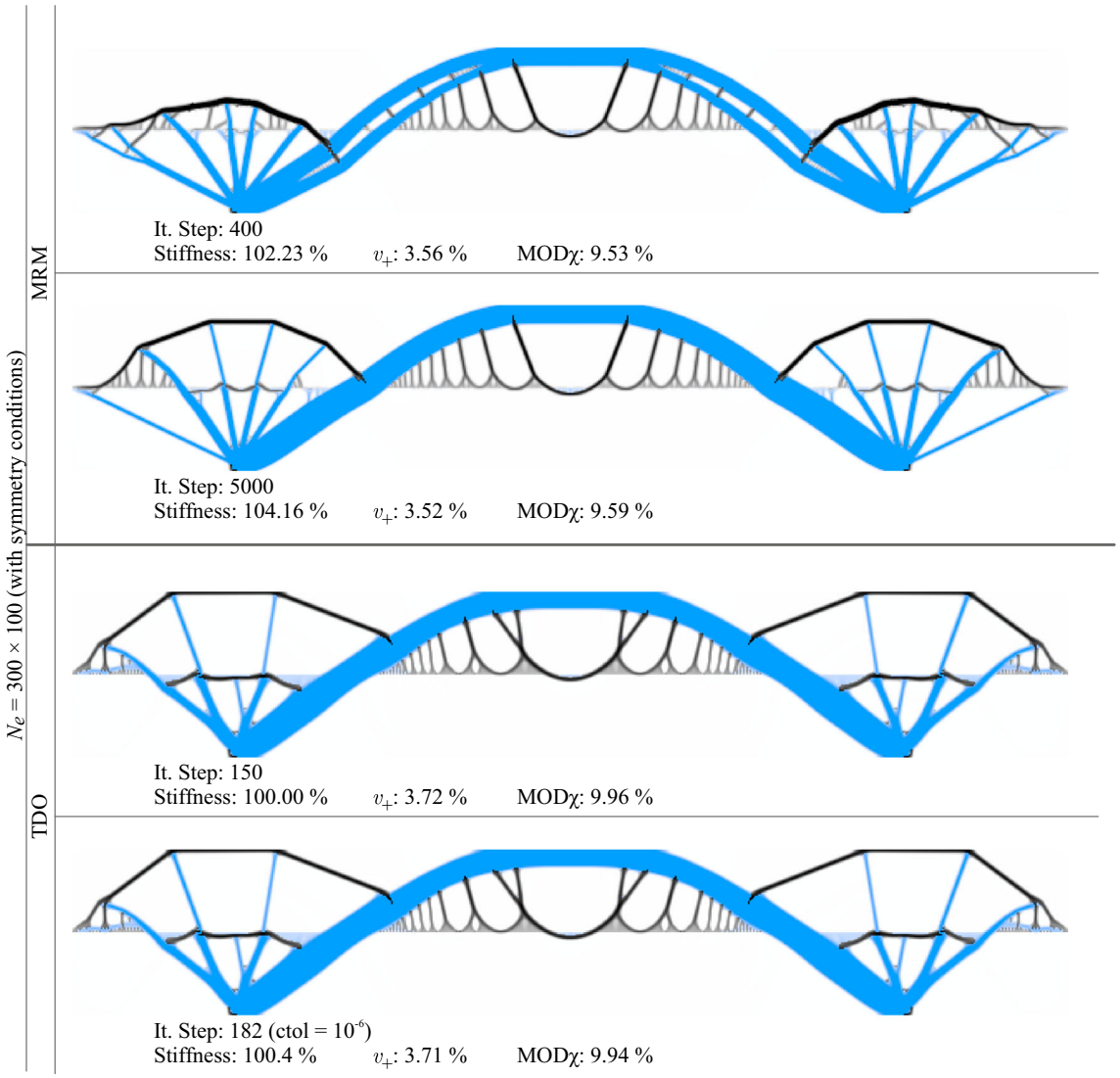

Fig. 24 Topologies obtained for the bridge-like problem with $h = 1/100$. Filter radius $r_{\min} = 1.5h$ for the MRM method and regularization parameter $\beta^* = 2.0h^2$ for the TDO method

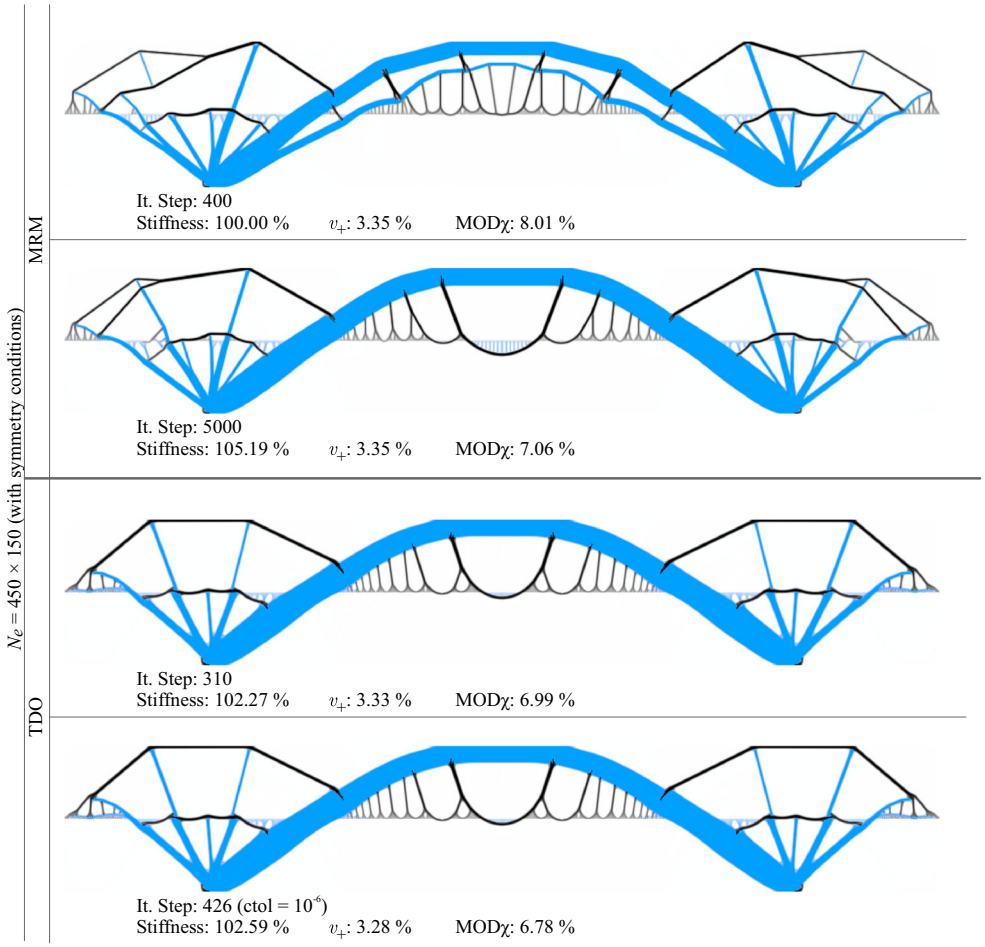

Fig. 25 Topologies obtained for the bridge-like problem with $h = 1/150$. Filter radius $r_{\min} = 1.5h$ for the MRM method and regularization parameter $\beta^* = 2.0h^2$ for the TDO method

load cases. The sensitivities of each load case are weighted likewise. To this end, the FE calculations for each load case are carried out separately with the current design variables, which results in different weighted sensitivities for each load case. The resulting weighted sensitivities are summed up for a single optimization step, which combines all load cases.

This procedure can also be applied for the MRM by replacing the modified sensitivities given in (22) and (23) by the sum of the weighted modified sensitivities over all load cases, provided that the spectral decomposition of the stress is performed separately for each load case. For the TDO, the procedure can be performed analogously by replacing the driving forces (47) and the time derivative (49) by their respective sum over all load cases. Additionally, the viscosity η_φ is multiplied by the number of load cases to maintain the numerical damping and evolution speed of the phase variable. The viscosity η_χ is automatically adjusted by applying the sum of the driving forces over all load cases in (53). Figures 26 and 27 show two examples in which the two loads are applied as single and multiple load cases. All load cases are weighted equally.

The example given in Fig. 26 shows the requirement of multiple load cases: if the forces are applied as one load case, no connection to the supports is established due to the (vertical) equilibrium of the forces. If the forces would be applied as separated load cases, the structure would fail. For the single load cases, the MRM and TDO yield very similar results, whereas the multiple load cases differ partially. In the first example given in Fig. 26, the MRM yields compression affine material in the trusses on the right; whereas, the TDO yields a composite of tension and compression affine material. The structural stiffness for the TDO is higher, which is mainly provided by the larger amount of stiffer tension affine material used in the design. The second example is given in Fig. 27. The frame bracing is made of the stiffer tension affine material in both results. In MRM, the node connecting the tension struts is on the bottom of the design space; whereas in TDO, it is oriented towards the center. The two

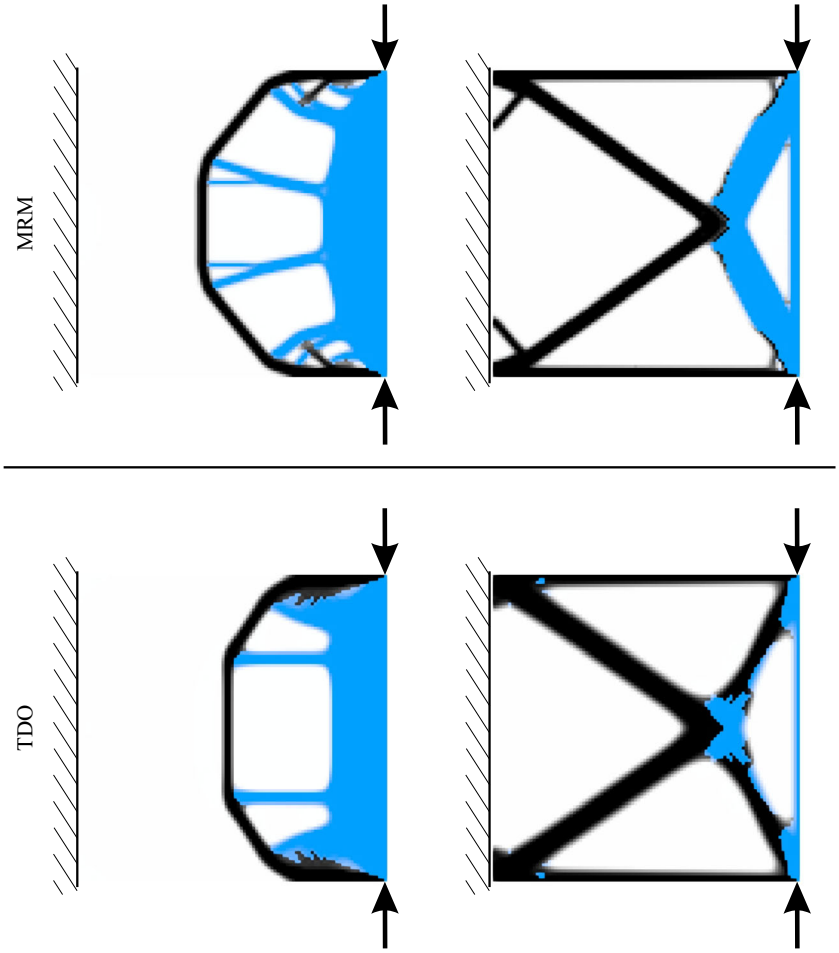

Fig. 26 Example for the application of two loads as single load case (left) and multiple load cases (right)

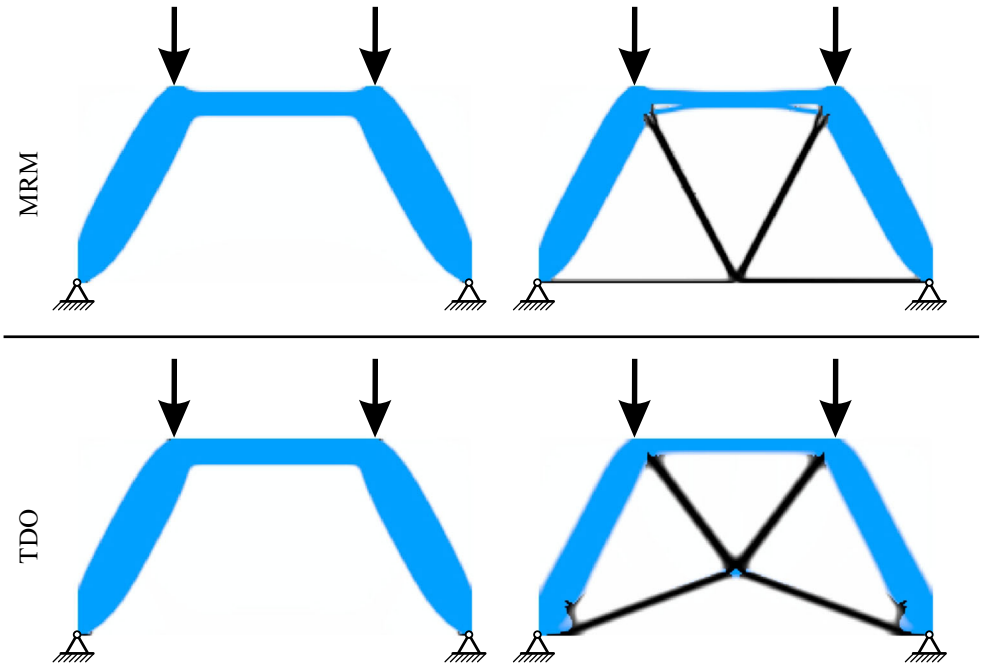

Fig. 27 Example for the application of two loads as single load case (left) and multiple load cases (right)

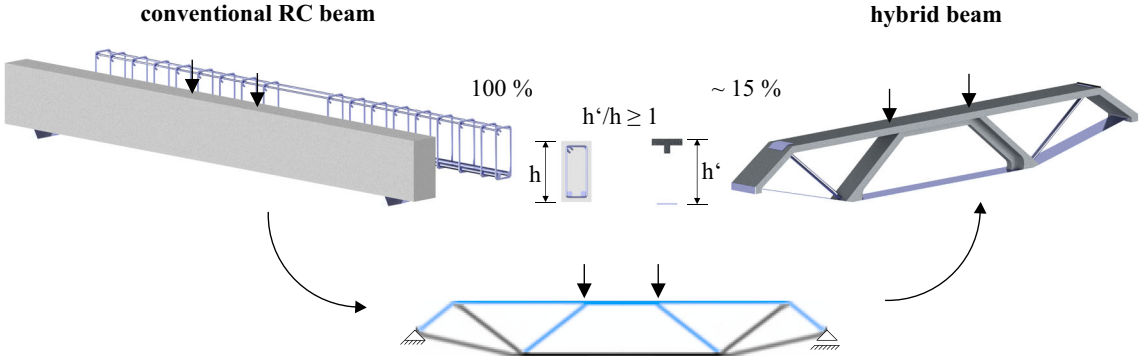

Fig. 28 Transformation of a conventionally reinforced concrete beam to a weight-optimized hybrid concrete-steel beam by topology optimization

multiple load case examples reveal an interesting aspect in tension/compression anisotropy enhanced topology design. For instance, regarding Fig. 27, if the load on the right side is active, the truss between the lower left and the upper right supports the load in a compressive state, whereby the other diagonal structural member is under tensile stress. For the other load case, i.e., the load on the left side is active, the opposite applies. Therefore, it is to say, that there is no actually suitable material for these structural members due to the changing stresses. However, in order to maximize the weighted average of the structural stiffness, the stiffer material (steel) is employed. The examples show that further investigations related to incorporating multiple load cases within a multi-material optimization problem that tackles the tension/compression anisotropy of materials are worth to be accounted. However, this is beyond the scope of this publication and has to be investigated carefully in future research efforts.

7 Practical application

Although concrete can be casted in nearly any shape, this benefit is poorly used in practical application. In recent years, some research effort has been done in civil engineering, concerning for example optimized reinforcement (Putke and Mark 2014; Putke et al. 2015, 2016; Schmidt-Thrö et al. 2018;) and parabolic trough collectors (Forman et al. 2016; Kämper et al. 2017). However, still concrete beams and plates with compact cross sections are designed often, hence leading to oversized structural components. Simple improvements concerning the general shape, cross-section layout, and material distribution ensure weight-optimized structures with equivalent load-bearing capacity. The presented method for tension/compression anisotropy enhancement enables the feasibility to perform an adequate topology optimization taking into account the characteristic requirements existing in structural engineering. As mentioned in the introduction, the objective in concrete design is to exploit the benefits of both materials, i.e., concrete and structural steel. While concrete is comparatively lightweight, economical and has high compressive strength, it can barely sustain tensile stresses. In comparison, steel has an equally high compressive and tensile strength but suffers from a high density and material price. Thus, the proposed methods could be used to reduce the cost of materials and structural weight considerably by arranging material only where really needed. In Fig. 28 a conventional concrete beam with rectangular cross-section and accompanying longitudinal reinforcement for bending and stirrups for the internal shear force is shown. Modeling the 4-point bending problem with FE and applying one of the proposed methods (here exemplary MRM), the material distribution can be optimized in such a way that the structural volume, weight and costs are decreased drastically. Further material reduction can be attained by increasing the height of the predefined design space. Eventually, UHPC with its much higher compressive strength can be utilized to minimize the material costs even further to about 15% relative to the initial beam volume. As a consequence of the optimization procedure, a hybrid concrete-steel beam results in which no redundant material is employed. The structural layout and material distribution is designed to transform bending in axial loads and thus bear loads most effectively.

8 Conclusion and outlook

A general idea to the tension/compression anisotropy enhancement to topology design was presented. To this end, a three-phase (two solid and one void material) system, distinguishing between materials' tensile and compressive stress affinity, has been introduced along with an energetic measure for the tension and the compression affine material. The implementation of this enhancement to topology optimization was demonstrated using two different optimization schemes: the extended material-replacement method (MRM) which applies modified stiffness matrices for the

optimization based on MMA, and the thermodynamic topology optimization (TDO) which applies Hamilton's principle with additional energetic penalization to derive evolution equations for the design update. Although the tension/compression anisotropy enhancement was implemented into different topology optimization approaches, similar results are obtained. Surely, both optimization schemes can be improved further in future works. For example, more sophisticated filter techniques for the density variable or filter techniques for the phase distribution could be included to improve the convergence behavior or to apply manufacturing constraints. However, the computed results demonstrate the applicability in practice already. Furthermore, it is planned to construct and test experimentally the proposed optimized hybrid concrete-steel structures shortly and verify their superiority over conventionally designed RC counterparts.

References

Andreassen E, Clausen A, Schevenels M, Lazarov BS, Sigmund O (2011) Efficient topology optimization in matlab using 88 lines of code. Struct Multidiscip Optim 43(1):1–16

Bendsøe MP (1989) Optimal shape design as a material distribution problem. Struct Optim 1(4):193–202

Bendsøe MP, Kikuchi N (1988) Generating optimal topologies in structural design using a homogenization method. Comput Methods Appl Mech Eng 71(2):197–224

Bendsøe MP, Sigmund O (1999) Material interpolation schemes in topology optimization. Arch Appl Mech 69(9-10):635–654

Bruggi M, Duysinx P (2012) Topology optimization for minimum weight with compliance and stress constraints. Struct Multidiscip Optim 46(3):369–384

Cai K (2011) A simple approach to find optimal topology of a continuum with tension-only or compression-only material. Struct Multidiscip Optim 43(6):827–835

Cai K, Cao J, Shi J, Liu L, Qin QH (2016) Optimal layout of multiple bi-modulus materials. Struct Multidiscip Optim 53(4):801–811

De Borst R, Mühlhaus H-B (1992) Gradient-dependent plasticity: formulation and algorithmic aspects. Int J Numer Methods Eng 35(3):521–539

Diaz A, Sigmund O (1995) Checkerboard patterns in layout optimization. Struct Optim 10(1):40–45

Engl HW, Kunisch K, Neubauer A (1989) Convergence rates for tikhonov regularisation of non-linear ill-posed problems. Inverse Prob 5(4):523

Forman P, Kämper C, Stallmann T, Schnell J, Mark P (2016) Parabolic shells made from high-performance concrete for solar collectors. Beton- und Stahlbetonbau 111(2):851–861

Jantos DR, Junker P, Hackl K (2016) An evolutionary topology optimization approach with variationally controlled growth. Comput Methods Appl Mech Eng 310:780–801

Jantos DR, Hackl K, Junker P (2018a) An accurate and fast regularization approach to thermodynamic topology optimization. Int J Numer Methods Eng. https://doi.org/10.1002/nme.5988

Jantos DR, Junker P, Hackl K (2018b) Optimized growth and reorientation of anisotropic material based on evolution equations. Comput Mech 1–20. https://doi.org/10.1007/s00466-017-1483-3

Junker P (2014) A novel approach to representative orientation distribution functions for modeling and simulation of polycrystalline shape memory alloys. Int J Numer Methods Eng 98(11):799–818

Junker P, Hackl K (2015) A variational growth approach to topology optimization. Struct Multidiscip Optim 52(2):293–304

Junker P, Hackl K (2016) A discontinuous phase field approach to variational growth-based topology optimization. Struct Multidiscip Optim 54(1):81–94

Junker P, Schwarz S, Jantos DR, Hackl K (2019) A fast and robust numerical treatment of a gradient-enhanced model for brittle damage. https://doi.org/10.1615/IntJMultCompEng.2018027813

Junker P, Schwarz S, Makowski J, Hackl K (2017) A relaxation-based approach to damage modeling. Contin Mech Thermodyn 29(1):291–310

Kämper C, Forman P, Stallmann T, Ahrens MA, Mark P, Schnell J (2017) Optimised high-performance concrete shells for parabolic trough collectors, Journal of the International Association for Shell and Spatial Structures (J. IASS) 58 (No. 1 March n. 191)

Liu S, Qiao H (2011) Topology optimization of continuum structures with different tensile and compressive properties in bridge layout design. Struct Multidiscip Optim 43(3):369–380

Luo Y, Kang Z (2012) Topology optimization of continuum structures with drucker–prager yield stress constraints. Comput Struct 90:65–75

Luo Y, Wang MY, Zhou M, Deng Z (2012) Optimal topology design of steel–concrete composite structures under stiffness and strength constraints. Comput Struct 112:433–444

Martinez P, Marti P, Querin O (2007) Growth method for size, topology, and geometry optimization of truss structures. Struct Multidiscip Optim 33(1):13–26

Mori T, Tanaka K (1973) Average stress in matrix and average elastic energy of materials with misfitting inclusions. Acta metallurgica 21(5):571–574

Peerlings RHJ, De Borst R, Brekelmans WAM, De Vree JHP (1996) Gradient enhanced damage for quasi-brittle materials. Int J Numer Methods Eng 39(19):3391–3403

Putke T, Bergmeister K, Mark P (2016) Wirtschaftliches Konstruieren und Bewehren. Betonkalender 2016:695–739

Putke T, Bohun R, Mark P (2015) Experimental analyses of an optimized shear load transfer in the circumferential joints of concrete segmental linings. Struct Concr 16(4):572–582

Putke T, Mark P (2014) Strut-and-tie modelling with topological optimisation. Beton- und Stahlbetonbau 109(9):618–627

Querin OM, Victoria M, Martí P (2010) Topology optimization of truss-like continua with different material properties in tension and compression. Struct Multidiscip Optim 42(1):25–32

Rojas-Labanda S, Sigmund O, Stolpe M (2017) A short numerical study on the optimization methods influence on topology optimization. Struct Multidiscip Optim 56(6):1603–1612

Rozvany G (2009) A critical review of established methods of structural topology optimization. Struct Multidiscip Optim 37(3):217–237

Schmidt-Thrö G, Tabka B, Smarslik M, Scheufler W, Fischer O, Mark P (2018) Experimental investigations of partial loading capacity with plane load distribution. Beton- und Stahlbetonbau 113(2):115–126

Sigmund O (1997) On the design of compliant mechanisms using topology optimization. Mech Struct Mach 25(4):493–524

Sigmund O (2001a) A 99 line topology optimization code written in matlab. Struct Multidiscip Optim 21(2):120–127

Sigmund O (2001b) Design of multiphysics actuators using topology optimization – part ii: Two-material structures. Comput Methods Appl Mech Eng 190(49-50):6605–6627

Sigmund O (2007) Morphology-based black and white filters for topology optimization. Struct Multidiscip Optim 33(4):401–424

Sigmund O, Maute K (2013) Topology optimization approaches. Struct Multidiscip Optim 48(6):1031–1055

Sigmund O, Petersson J (1998) Numerical instabilities in topology optimization: a survey on procedures dealing with checkerboards, mesh-dependencies and local minima. Struct Optim 16(1):68–75

Stolpe M, Svanberg K (2001) On the trajectories of penalization methods for topology optimization. Struct Multidiscip Optim 21(2):128–139

Svanberg K (2007) MMA and GCMMA - two methods for nonlinear optimization, Optimization and Systems Theory, KTH, Stockholm (Sweden)

Svanberg K (1987) The method of moving asymptotes - a new method for structural optimization. Int J Numer Methods Eng 24(2):359–373

Voyiadjis GZ, Taqieddin ZN, Kattan PI (2008) Anisotropic damage–plasticity model for concrete. Int J Plast 24(10):1946–1965

Wang MY, Zhou S (2004) Phase field: a variational method for structural topology optimization. Comput Model Eng Sci 6(6):547–566

Yamada T, Izui K, Nishiwaki S, Takezawa A (2010) A topology optimization method based on the level set method incorporating a fictitious interface energy. Comput Methods Appl Mech Eng 199(45-48):2876–2891